

國立交通大學

電機與控制工程學系

碩士論文

雙窗法用於指甲襞微血管之血流速度的分析

Analysis of Nailfold Capillary Blood Velocity by

Dual-Windows Method

研究生：林恩榮

指導教授：羅佩禎 博士

中華民國九十七年二月

雙窗法用於指甲襞微血管之血流速度的分析  
Analysis of Nailfold Capillary Blood Velocity by  
Dual-Windows Method

研究生：林恩榮

Student : En-Jung Lin

指導教授：羅佩禎 博士

Advisor : Dr. Pei-Chen Lo

國立交通大學

電機與控制工程學系

碩士論文

A Thesis

Submitted to Department of Electrical and Control Engineering

College of Electrical and Computer Engineering

National Chiao Tung University

In Partial Fulfillment of the Requirements

For the Degree of

Master

In

Electrical and Control Engineering

February 2008

Hsinchu, Taiwan, Republic of China

中華民國九十七年二月

# 雙窗法用於指甲襞微血管之血流速度的分析

研究生：林恩榮

指導教授：羅佩禎 博士

國立交通大學電機與控制工程學系

## 摘要

微循環是人體的一個重要的功能性機制並且透過顯微觀察可以顯示出人體的生理狀態。對於某些設計實驗而言，這個生理參數可以提供非常有用的資訊。本研究的目的是藉著顯微技術來開發一個可靠的方法去觀察微循環的變化與反應。雙窗法是根據動態影像來估測微血管血流速度的一種可行的方法。在本研究中我們詳細地討論影像處理方法以及闡述如何去選擇某些分析上的重要參數。最後我們將雙窗法應用在 4 位受測者，包括 2 位具有禪坐經驗者，以及 2 位無禪坐經驗受測者為控制組。由結果發現，實驗組的微血管血流速度較控制組的來的高。而根據血液動力學，較高的血流速度的成因是較低的血管阻力、較佳的血管彈性以及較低的血液黏滯度。因此推測長時間練習禪坐的人在微循環系統上有較好的效率表現。


# **Analysis of Nailfold Capillary Blood Velocity by Dual-Windows Method**

**Student : En-Jung Lin**

**Advisor :Dr. Pei-Chen Lo**

**Institute of Electrical and Control Engineering  
National Chiao-Tung University**

## **Abstract**



Microcirculation is an important functional mechanism of human body and it reveals physiological states of the human body down to the microscopic details. It thus provides a feasible tool to characterize some control experiments. The aim of this study is to develop a reliable scheme for investigating microcirculation behavior based on microscopic image technology. Dual-windows method is particularly feasible for estimating the capillary blood velocity based on motion pictures. In the thesis, we discussed in details the methods of image processing and analysis and elucidated how to make an appropriate choice of some important parameters. Finally, we applied the proposed scheme to 4 subjects, 2 Zen-meditation practitioners and 2 control subjects. The results indicated that meditation practitioners had much higher capillary blood velocities. According to hemodynamics, higher blood velocity might be resulted from smaller blood-vessel resistance, better vessel elasticity, or low blood viscosity. Therefore we might conjecture that people who practice meditation for a long time exhibit better efficiency in their microcirculatory system.

## 誌 謝

這篇論文的完成，首先要感謝指導教授羅佩禎老師的指導，對於我這種右腦思考的人，老師所給予的科學訓練是非常有幫助的，此外在英文論文寫作方面也給予我多方的幫助與教導，在此表達對老師的謝意。同時也要感謝口試委員胡竹生、黃聖傑老師對於論文提出的指導和建議。

在碩士班的研究生涯中，我要特別感謝權毅學長對於論文的方向、方法與寫作上的熱心指導，以及適達學長對論文校改的辛勞。也感謝晏銘、憲正、政勳、進忠、偉凱學長、瑄詠學姊在這段時間給了我許多研究上的建議和鼓勵。在程式撰寫方面，特別感謝政恩、我的大學同學建樟及老前輩洪國智大哥，沒有他們論文不會這麼順利完成。還有謝謝一起努力的博翔、宗仁、信丞、昶毅。另外，也感謝學弟 buwonol 讓我能夠練習英文、嘉鴻為實驗室帶來的歡樂氣氛、啦啦隊的瑤瑤與小游及各位隊友，讓我的研究生涯過得相當充實。

最後我要感謝父母和家人們，謝謝你們持續的關心和支持，讓我能夠在沒有後顧之憂下完成學業。

# Contents

中文摘要.....	i
Abstract.....	ii
誌謝.....	iii
Contents.....	iv
List of Tables.....	vii
List of Figures.....	viii
<b>1. Introduction.....</b>	<b>1</b>
1.1 Introduction to Microcirculation.....	1
1.1.1 Structure of Microcirculation.....	1
1.1.2 Physiological Function of Microcirculation.....	2
1.2 Motivation and Aim of this Thesis.....	3
1.2.1 Motivation.....	3
1.2.2 Aim of this Thesis.....	5
1.3 Organization of this Thesis.....	5
<b>2. Theory and Methods.....</b>	<b>6</b>
2.1 Methods for Capillary Blood Velocity Measurement.....	6
2.2 Theory of the Dual-Windows Method.....	9
2.2.1 Background of the Dual-Windows Method.....	9
2.2.2 Theory of Dual-Windows Method.....	9
<b>3. Experiment Set-up and Preprocessing of the Capillary</b>	
<b>Mircoscopic Image.....</b>	<b>12</b>
3.1 Introduction to Nailfold.....	12

3.2 Experimental Set-up.....	14
3.2.1 Instruments .....	14
3.2.2 Physical Dimension of One Pixel in Microscopic Image .....	16
3.2.3 Experimental Subjects.....	19
3.2.4 Experimental Environment .....	19
3.2.5 Experimental Procedure .....	19
3.3 Enhancement of Microscopic Capillary Image .....	21
3.4 Dynamic Microscopic Image Realignment .....	24
3.4.1 Block Matching Algorithm .....	25
3.4.2 Matching criteria.....	26
3.5 Segmentation and Skeletonization of Microscopic Capillary Images .....	27
3.5.1 Segmentation.....	27
3.5.2 Skeletonization.....	28
3.6 Procedure of Estimating Capillary Blood Velocity .....	29
<b>4. Results .....</b>	<b>32</b>
4.1 Effects of Instrumentation Setting on Image Quality .....	32
4.2 Issue of Realignment.....	38
4.2.1 Comparison Between Two Methods for Realignment .....	38
4.2.2 A Greater Error in Realignment.....	41
4.3 Morphological Approach for Locating Observation Windows.....	42
4.4 Estimation of Capillary Blood Velocity .....	44
4.4.1 Estimate of Capillary Blood Velocity by Finding the Center of Blood Cell .....	44
4.4.2 Estimate of Capillary Blood Velocity by Proposed Scheme .....	45
<b>5. Conclusion and Discussion .....</b>	<b>52</b>
5.1 Conclusion and Discussion of Current Study .....	52

5.2 Future Work ..... 54

**References.....56**

**Appendix A. Other Matching Criteria .....60**

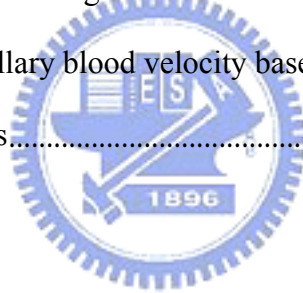
**Appendix B. Otsu’s Method .....61**





# List of Tables

2.1 Advantages and disadvantages of the three methods .....	9
3.1 Specifications for microscope .....	14
3.2 Specifications for frame-grabbing card .....	15
3.3 Horizontal scale mapping of physical length of one pixel.....	18
3.4 Vertical scale mapping of physical length of one pixel.....	18
3.5 Mean and SD (standard deviation) of physical length of one pixel.....	18
3.6 Subjects of experimental and control groups .....	19
4.1 Number of shifted pixels used to generate ten shifting images.....	40
4.2 The 100 estimates for capillary blood velocity based on 100 non-overlapping frame sets.....	48



# List of Figures

1.1 Network of microcirculation.....	2
2.1 Two microscopic images acquired from: (a) frame k (b) frame k+1 .....	7
2.2 A pair of capillary images: (a)frame k (b) frame k+1 .....	8
2.3 Resulted <i>velocity flow field</i> of blood cells.....	8
2.4 A microscopic image with Window A and Window B.....	10
2.5 Average gray levels varying with time evaluated from pixels within:	
(a) Window A (b) Window B.....	10
3.1 Nailfold region on the finger .....	13
3.2 Cross-section of nailfold .....	13
3.3 Microscope for microcirculation data collection.....	14
3.4 Image of capillaries captured by RT4 VGuard frame-grabbing card.....	15
3.5 Objective micrometer .....	16
3.6 Demonstration of scale (a) horizontal and (b) vertical.....	17
3.7 Experimental procedure .....	19
3.8 Original microscopic image of microcirculation.....	21
3.9 The strategy of preprocessing.....	22
3.10 (a) Raw image, (b) R-plate image, (c) G-plate image, and (d) B-plate image .....	23
3.11 Illustration of block matching .....	25
3.12 Capillary image (a) before segmentation (gray-scale image), and (b) after segmentation (binary image)).....	27
3.13 (a) Binary capillary image before skeletonization, and (b) blood-flow	

pathway derived by skeletonization.....	28
3.14 Procedure of estimating CBV by dual-windows method .....	29
3.15 A diagram of the two chosen windows.....	30
3.16 Average gray level plotted against time.....	30
4.1 Schematic illustration for illumination source from (a) upper back, and (b) upper front of the finger.....	33
4.2 Images acquired by illumination locating at (a) upper back, and (b) upper front of the finger .....	34
4.3(a) R-plate, (b) Histogram of R-plate image, (c) G-plate, (d) histogram of G-plate, (e) B-plate, and (f) histogram of B-plate .....	35
4.4 White-squared segment of (a) G-plate image, and (b) B-plate image in Figures 4.3(c) and 4.3(e), respectively .....	36
4.5 Histogram of (a) Figure 4.4(a), and (b) Figure 4.4(b).....	36
4.6 (a) G-plate image, (b) histogram of block A (background, size: 30x30), (c) histogram of block B (capillary, size: 5x5), and (d) histogram of block C (capillary, size: 5x5).....	37
4.7 Binary images derived from (a) G-plate component, and (b) B-plate component .....	38
4.8 (a) Original image, and (b) shifted image (shifted downward).....	39
4.9 (a) Error in realignment using Method 1, and (b) error in realignment using Method 2 .....	40
4.10 Image frames selected from the same video: (a) the 1491 <sup>st</sup> frame, and (b) the 1 <sup>st</sup> frame.....	41
4.11 (a) Original image, (b) skeleton image, and (c) overlapping image .....	42
4.12 Illustration of insufficient distance between two observation windows.....	43

4.13 Capillary image of (a) the 167<sup>th</sup> frame, and (b) the 168<sup>th</sup> frame .....44

4.14 (a) Initial positions of two windows, and (b) desired positions of two windows with Window A descending .....46

4.15 The one second, gray-level variations inside Window A and Window B using (a) the initial window positions, and (b) the modified window positions with double in-between distance .....46

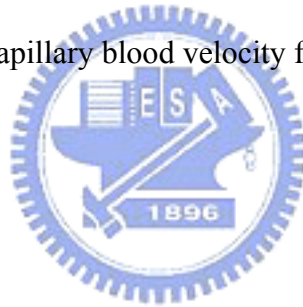
4.16 The 100 estimates for capillary blood velocity based on 100 non-overlapping frame sets.....48

4.17 Estimate of one-minute capillary blood velocity for experimental subject 1 ...49

4.18 Estimate of one-minute capillary blood velocity for experimental subject 2 ...49

4.19 Estimate of one-minute capillary blood velocity for control subject 1 .....50

4.20 Estimate of one-minute capillary blood velocity for control subject 2 .....50

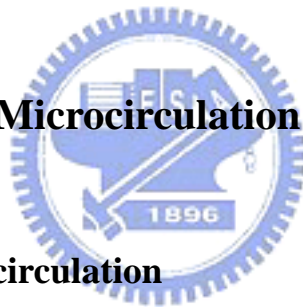


# Chapter 1

## Introduction

Circulation is an important mechanism for the human life. Systemic circulation and pulmonary circulation are examples of large-scale circulation systems that are mostly studied by medical and engineering professionals. Recently, the smallest circulation system, microcirculation, has drawn the attention of researchers and medical experts since its role in predicting and diagnosing a number of disease [1–3]. In this chapter, we will firstly illustrate the structure of microcirculation and how it works.

### 1.1 Introduction to Microcirculation



#### 1.1.1 Structure of Microcirculation

Microcirculation system is the smallest unit in human body circulatory system. The main function of this system is exchanging body fluid through blood vessels of arteriole, capillary, venule and etc.. Blood flows from larger blood vessels to smaller ones in the order of arteriole, precapillary, metarterioles, capillary, and finally venule. This network of circulation is illustrated in Figure 1.1.

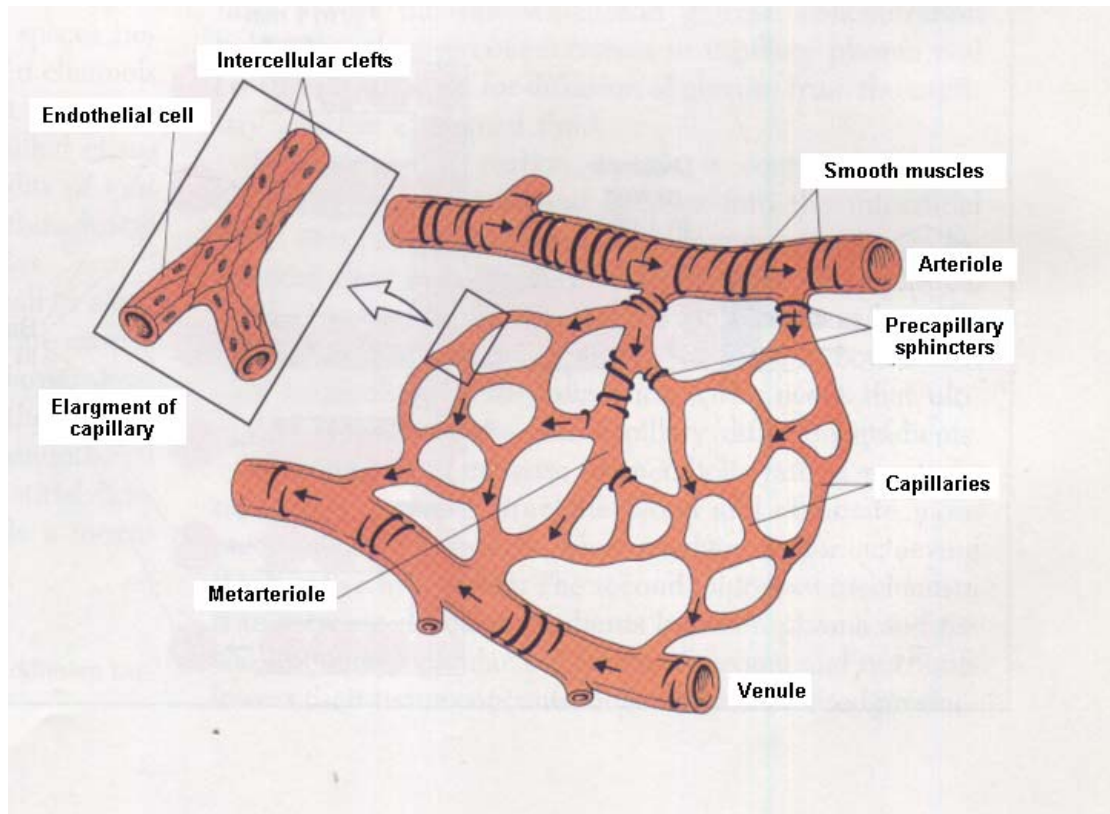


Figure 1.1 Network of microcirculation [4].

### 1.1.2 Physiological Function of Microcirculation

Although there is only 5% of blood in microcirculation, it is the most important circulation in a human body due to its major role in substance exchange. Three main physiological functions of microcirculation are depicted as follows:

#### 1. *Transportation and exchange of substances*

This is a basic function of microcirculation. As blood flows into a capillary bed, nutrients, gases, water, and hormones carried by blood immediately diffuse out of the tiny thin-walled vessels. Meanwhile, water-dissolvable wastes in the tissues, such as carbon dioxide, begin to diffuse inward.

#### 2. *Communication among tissues and cells*

Because microcirculation allows effective exchange of substances, substances of one tissue can be transported to another far-away tissue. This procedure of

transportation is one of the important and fundamental mechanisms for homeostasis maintenance inside the human body.

### *3. Control of blood flow*

For some small vessels like arterioles and venules, the diameter can contract or expand by their smooth muscles to change the blood flow of microcirculation.

## **1.2 Motivation and Aim of this Thesis**

### **1.2.1 Motivation**

Circulatory system manipulates the core physiological condition of a human body. Therefore, it is an important issue in human physiology and clinical pathology. Due to the progress of biomedical engineering, more and more electronic devices like “Laser Doppler Anemometer” have been developed to observe and measure body fluid circulation [5, 6]. As a consequence, lots of scientific data of significance have been accumulated.

The microcirculation of nailfold has been studied in numerous fields of medical science. In the neonate field, Norman et al. [7] proposed a study about neonate and capillary. They used a computerized videophotometric method to investigate the neonate’s capillary blood velocity. They found that the neonate’s capillary blood velocity is not different from the adult’s capillary blood velocity. In immunology, Aubin et al. [1] studied the relationship between nailfold capillary microscopy (NCM) and advanced HIV patients. With the use of NCM, it was found that advanced HIV patients had more abnormal capillaries than normal people. Moreover, this research also confirmed that the significant capillary abnormalities could be detected in the same type of patients using NCM, although they did not present any cutaneous or

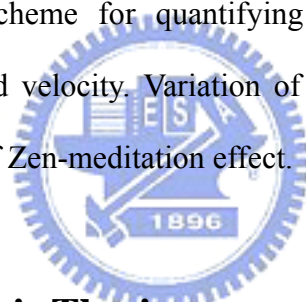
systemic symptoms of vasculitis. In hemodynamics, Drewe et al. [2] studied the effects of specific drugs on hypertensive patients by means of capillary blood velocity. It was found that the capillary blood velocity increases after the essential hypertensive patients taking the antihypertensive drug called “Enalapril”. In radiology, Brumen et al. [3] found that nailfold capillaroscopy is one of the methods suitable for diagnosis of vascular radiolesions in subjects occupationally exposed to ionizing radiation. In chronic disease, Chinese researchers have found that many diseases revealed microcirculation abnormality even before the obvious symptoms of the diseases occurred [8, 9]. For example, there are significant differences on microcirculation characteristics between insulin-dependent diabetes mellitus (IDDM) patients and non-insulin-dependent diabetes mellitus (NIDDM) patients [9]. In short, the above research over the last twenty years or so indicates the growing importance of nailfold capillary microscope in the wider context.

As a comparison, in Taiwan, although research has been conducted in the area of blood circulation, much still remains to be done in order for it to reach the level achieved elsewhere. More specifically, most research in Taiwan has focused on large or medium blood vessels. Microcirculation, however, has only become a focus topic in the last ten years and only in a few theses. Furthermore almost all of those theses have focused on technically improving the measurement of capillary blood velocity [10]; however, few have discussed the relationship between health condition and capillary blood velocity [6, 11]. In summary, this thesis, inspired by the studies outside Taiwan, seeks to observe the effects of capillary blood velocity on people who practice Zen-meditation.



## **1.2.2 Aim of this Thesis**

As described above, microcirculation reveals physiological states of the human body down to the microscopic details. It thus can provide a feasible tool to characterize some control experiments. For example, our research group has been investigating the human life model under Zen meditation since 1998, mainly focusing on such electrophysiological signals like electroencephalograph (EEG), visual evoked potential (VEP), galvanometric skin resistance (GSR), and electrocardiograph (ECG). According to the analysis of former data, we decided to further investigate microcirculation behavior for Zen-meditation practitioners. This preliminary study was aimed to develop a scheme for quantifying microcirculation behavior by estimating the capillary blood velocity. Variation of capillary blood velocity would then be applied to the study of Zen-meditation effect.



## **1.3 Organization of this Thesis**

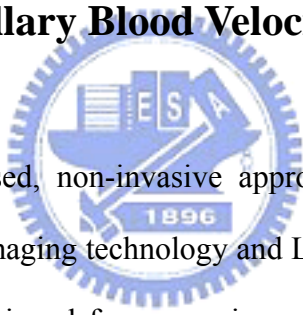
This thesis is composed of five chapters. Chapter 1 introduces the microcirculation as well as the motivation and main aim of this study. In Chapter 2 depicts the theory of dual windows method and the algorithm for estimating capillary blood velocity. Chapter 3, experimental setup and procedure are presented. In addition, method for microscopic image preprocessing is described. Chapter 4 reports and discusses the results. The last chapter makes a summary of this research and brings forward some issues for future study.

# Chapter 2

## Theory and Methods

In the study of microcirculation, a number of methods and instruments have been developed and employed in measuring the capillary blood velocity. In the beginning of this chapter, three commonly used methods are introduced. Section 2.2 describes the theory and method used in this study.

### 2.1 Methods for Capillary Blood Velocity Measurement



There exist two widely used, non-invasive approaches for measuring capillary blood velocity, microscopic-imaging technology and Laser-Doppler anemometer [12]. The former is particularly designed for measuring microscopic, individual-capillary blood velocity from the nailfold capillary bed. In addition to scrutinizing the movement of the blood cell directly on an LCD screen, this approach provides the advantage of viewing the capillary shape that has been used to diagnose some potential abnormalities. On the other hand, Laser-Doppler anemometer is an instrument developed to detect the overall phenomenon of capillary blood flow within the laser-illuminated region. Due to the hypothesis that Zen meditation might affect microcirculation behavior, we therefore preferred employing the first approach to the study of local, microscopic blood flow phenomenon.

Three methods have been developed to measure the capillary blood velocity based on the microscopic imaging technology. We briefly describe them below.

### 1. Dual-windows method

This is the main method [13–15] adopted in the thesis. A brief description is provided here. Details are described in Section 2.2. Advantages of dual-windows method include fast processing and easy implementation. We only need to locate two observing windows and use a simple formula to estimate the capillary blood velocity.

### 2. Direct observation method

This method requires clear microscopic image so that the movement of blood cells can be observed by examination. As an illustration of this method, two microscopic images are shown in Figure 2.1. After the blood cells have been observed by the naked eye, the distance from the center of the blood cell in Frame  $k$  to the center of the blood cell in Frame  $k+1$  is computed and found to be  $\Delta d$ . The time interval of consecutive frames,  $\Delta t$ , is 1/30 second. Then the formula  $v = \frac{\Delta d}{\Delta t}$  is applied to calculate the capillary blood velocity.

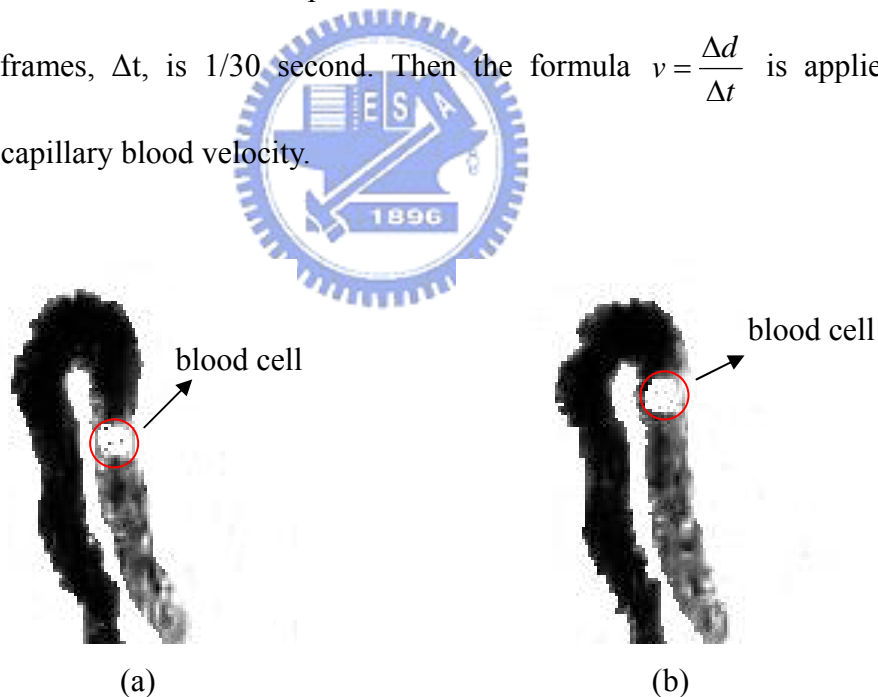


Figure 2.1 Two microscopic images acquired from (a) frame  $k$ , and (b) frame  $k+1$ .

### 3. Optical flow method

Optical flow method [16, 17] is one of the methods in motion estimating. Motion estimation using optical flow method results the *velocity flow field* from a pair of images. As an illustration, Figure 2.3 displays two consecutive microscopic capillary images. The resulted *velocity flow field* of blood cells is shown in Figure 2.4. Each arrow represents the velocity vector of a blood cell inside the capillary.



Figure 2.2 A pair of capillary images: (a) frame k and (b) frame k+1.



Figure 2.3 Resulted *velocity flow field* of blood cells [11].

Table 2.1 provides a comparison of the three methods. We can see that the direct observation method needs very clear images, it increases the degree of difficult for measuring blood velocity. The optical flow method provides the most amount of

information of blood velocity in the capillary in the three methods. However, this method is time-consuming in computation. Therefore, we adopted the dual-windows method to derive the capillary blood velocity.

Table 2.1 Advantages and disadvantages of the three methods

Methods	Advantages	Disadvantages
Dual-Windows Method	Easy implementation and fast computation.	Upper limit of velocity detected is 2mm/sec due to finite image resolution.
Direct Observation Method	Immediate and direct.	Very clear images required and accuracy is not good.
Optical Flow Method	The blood velocity of every point in capillary (current velocity) can be measured.	Very extended computation time.



## 2.2 Theory of Dual-Windows Method

### 2.2.1 Background of Dual-Windows Method

In 1967, Wayland [18] proposed the method “dual slits” in order to inspect the microcirculation of the mesentery. This method is the forerunner of the dual-windows method. Later, the dual-windows method was proposed by Intaglietta [15]. In 2000, Tsukada [19] proposed a novel method that employed a circular window instead. The result was found to be more accurate than that estimated with a rectangular window.

### 2.2.2 Theory of Dual-Windows Method

The first step of dual-windows method is to choose a clear capillary from the serial microscopic images acquired by the computer. Within the region of chosen capillary, we define two observation windows of the same size as Window A and

Window B manually (see Figure 2.5) in which the average gray levels varying with time are inspected. Let  $G_a(t)$  and  $G_b(t)$  denote the average gray levels varying with time within Window A and Window B, respectively. Ideally,  $G_a(t)$  and  $G_b(t)$  should have a well-defined narrow peak as shown in Figure 2.6.

The rules of choosing the positions of the two windows are described in Section 4.3.



Figure 2.4 A microscopic image with Window A and Window B.

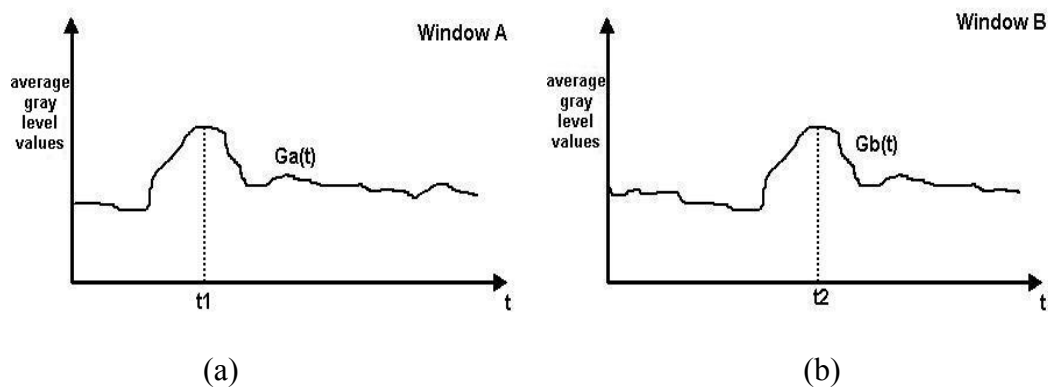


Figure 2.5 Average gray levels varying with time evaluated from pixels within (a) Window A, and (b) Window B.

According to Figure 2.5, direction of the blood flow was counterclockwise. The color of capillary was initially darker (smaller gray level) and became lighter when the blood cell passed through the window. As a result, the peak in  $G_a(t)$  (Figure 2.6(a)) indicates that the same blood cell detected by Window A at  $t_1$  flows through Window B at  $t_2$ . Based on these parameters, the capillary blood velocity can be evaluated using the formula:  $v = \frac{\Delta d}{\Delta t}$ , where  $\Delta d$  represents the distance between Window A and Window B, and  $\Delta t = t_2 - t_1$ . However, sometimes  $G_a(t)$  may not exhibit the same pattern in comparison with  $G_b(t)$ . Therefore, the cross correlation method was adopted to help determining the value  $\Delta t$  automatically.



# Chapter 3

## Experimental Set-up and Preprocessing of the Capillary Microscopic Image

This chapter introduces the background information, in three aspects, required to conduct the experiment. First of all, we present the reason for selecting the nailfold region as the subject of microscopic imaging in this study. Second, the specifications of the instruments and experimental procedure will be discussed in detail. Third, we illustrate the pre-processing scheme for manipulating poor microscopic image. External factors, such as background noise or finger movement, can easily and detrimentally affect the microscopic image. In addition, limitations of the resolution and sensitivity of the frame-grabbing card or the objective lens may result in microscopic image of poor quality. Therefore, preprocessing is a must in order to improve image quality. Thus, preprocessing methods used to improve image quality will be depicted in detail. Finally, substantial procedure for estimating capillary blood velocity is illustrated.

### 3.1 Introduction to Nailfold

Nailfold (see Figure 3.1) is the common and most suitable region for clinical microcirculation inspection. Most of the existing knowledge and understanding of clinical microcirculation is based on the results of nailfold microcirculation



inspections. Figure 3.2 shows a cross-section of the nailfold.

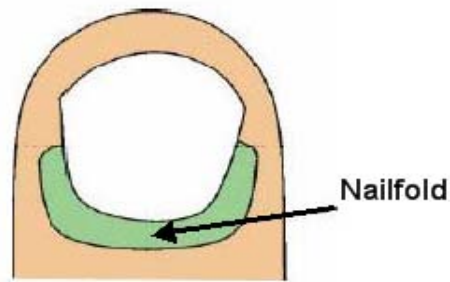


Figure 3.1 Nailfold region on the finger.

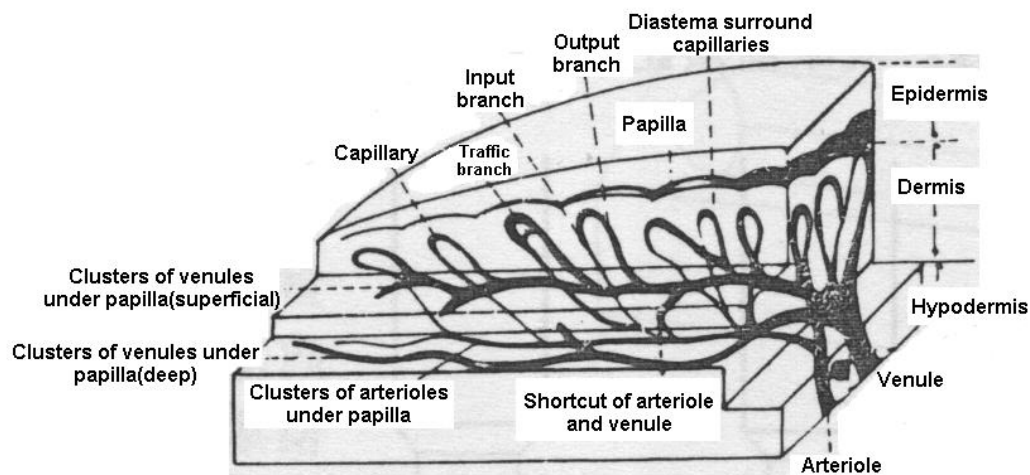


Figure 3.2 Cross-section of nailfold [8].

The reasons for choosing the nailfold region for observing microcirculation [8] are:

1. The epidermis of the nailfold region is thin and more penetrable by light. Therefore, the inspection of microcirculation can be non-invasive and safe.
2. The trend of capillaries in the nailfold region are nearly parallel (not vertical) to the epidermis. This makes the derivation of blood flow velocity more precisely.
3. There are more capillaries in the nailfold region compared with other parts of the human body.

4. Capillaries in this region are more sensitive to various kinds of stimulation.

## 3.2 Experimental Set-up

### 3.2.1 Instruments

#### 1. Microcirculation detection device

Table 3.1 lists the specifications for the microscope that satisfies our requirement.

Table 3.1 Specifications for microscope

Model:CCI-980	
Magnification	About 300X (in 15" LCD)
Finger platform	Can move 360°
Moving region of Platform	25*70mm
White balance	Auto
Light source	Side white LED light



Figure 3.3 Microscope for microcirculation data collection.

## 2. Frame-grabbing card

The specifications of frame-grabbing card we used are list in Table 3.2. By this card, an image of size 480×640 pixels can be obtained at a rate of 30 frames per second. An example image is shown in Figure 3.2.

Table 3.2 Specifications for frame-grabbing card

Model: RT4 VGuard digital video surveillance system	
Interface	32-bit PCI, grabbing continuous images
Resolution	In NTSC mode(640*480),30 frames per second
Channel	One card has four channels



Figure 3.4 Image of capillaries captured by RT4 VGuard frame-grabbing card.

### 3. Paraffin oil

Paraffin oil was used in order to reduce the degree of light reflection and provide clearer images.

### 4. Algorithm

Image processing algorithm was developed under MATLAB environment to estimate capillary blood velocity.

## 3.2.2 Physical Dimension of One Pixel in Microscopic Image

In order to calculate the capillary blood velocity, the physical dimension of one pixel in the microscopic image needs to be known. We thus employed the objective micrometer in estimating this length (Figure 3.5).



Figure 3.5 Objective micrometer.

The micrometer manufactured by a Japanese company has a circular viewing window with a small scale (1 mm). As the scale is too small for naked eyes, a microscope is used to measure the pixel level by taking the advantage of such a scale range.

Horizontal- and vertical-scale images (Figure 3.6) were used to estimate the physical length of one pixel. Then the mean value and standard variation of several measurements were calculated.

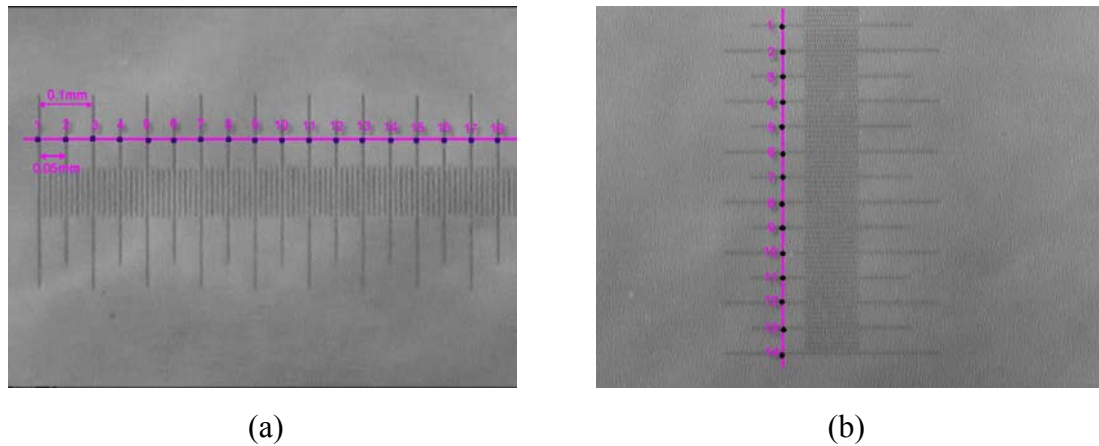


Figure 3.6 Demonstration of scale (a) horizontal and (b) vertical.

First, the micrometer image (480×640) was marked with a black dot at 0.0005m intervals on the scale. These assigned points were numbered 1–18 in the horizontal image and 1–14 in the vertical image. The locations of the points are shown in Table 3.3–3.5.

Table 3.3 Horizontal scale mapping of physical length of one pixel.

Index	1	2	3	4	5	6	7	8	9	10
Coordinate in pixel	39	73	113	141	175	209	243	277	311	345
Distance between two adjacent indexes (in pixel)	1-2	2-3	3-4	4-5	5-6	6-7	7-8	8-9	9-10	
	34	40	28	34	34	34	34	34	34	34
Index	11	12	13	14	15	16	17	18		
Coordinate in pixel	379	413	447	481	515	549	583	617		
Distance in pixel	10-11	11-12	12-13	13-14	14-15	15-16	16-17	17-18		
	34	34	34	34	34	34	34	34		

Table 3.4 Vertical scale mapping of physical length of one pixel.

NO.	1	2	3	4	5	6	7	8	9	10	11	12	13	14
coordinate	26	56	88	120	150	183	213	246	279	309	341	374	405	436
distance		1-2	2-3	3-4	4-5	5-6	6-7	7-8	8-9	9-10	10-11	11-12	12-13	13-14
		30	32	32	30	33	30	33	33	30	32	33	31	31

Table 3.5 Mean and SD (standard deviation) of physical length of one pixel.

Mean	Distance between two points
32.93pixel	0.05 mm
SD	The real length of one pixel
2.16 pixel	1.52 $\mu$ m

### 3.2.3 Experimental Subjects

This study involved two groups of subjects, the experimental group including subjects with Zen-meditation experience and the control group including subjects without any meditation experience. Background of subjects in each group is listed in Table 3.6.

Table 3.6 Subjects of experimental and control groups.

	Experimental group	Control group
Number of subjects	2	2
Sex	male	male
Age (years)	22, 26	27, 27
Meditation experience (years)	3, 7	

### 3.2.4 Experimental Environment

To best reduce the outside bias, experimental conditions like temperature, time and location were strictly controlled. All the experiments were conducted in the mid afternoon (around 3:30pm) in the Biomedical Signal Research Laboratory at NCTU.

### 3.2.5 Experimental Procedure

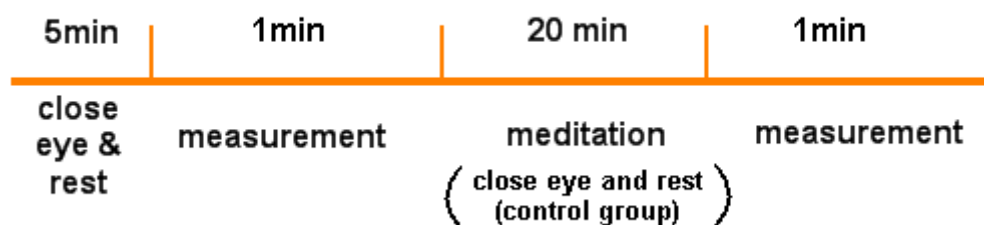


Figure 3.7 Experimental procedure.

The entire experimental procedure is illustrated in Figure 3.7. Details are described as follows:

1. First, subjects were asked to complete a personal data form and to take a standard DASS (Depression, Anxiety, Stress Scales) test to measure emotional state. The former involves questions concerning medical history, personal habits and attitudes towards such issues as drinking and smoking. The latter consists of 42 questions designed to elicit from the subject information about his/her emotional state during the week previous to the test date.
2. Second, subjects were required to rest for five minutes, with eyes closed. This is to remove other factors possibly affecting the physiological states of the subjects.
3. Third, paraffin oil was applied to the nailfold, and the middle finger was placed on the work plate on the microscope. The intensity, angle of incident, and focal distance of LED light were adjusted to capture a clear view of the capillaries.
4. Fourth, a frame-grabbing card was used to grab sequential images of the capillary. This process took 1 minute.
5. Finally, the experimental subjects took a meditation for 20 minutes, while the control subjects rested with eyes closed for the same duration. Afterwards, the capillary images were recorded again.

In image preprocessing, MATLAB facility was used to realign the shaking images, transform them to binary images, then skeletonize the images. The approximate middle line of skeleton image was identified and used to compute the capillary blood velocity.



### 3.3 Enhancement of Microscopic Capillary Image

The input source images  $\{f_0, f_1, f_2, \dots, f_n\}$  represent  $n$ 's continuous-frame images acquired from the microcirculation video data at 30 fps (frames per second). Accordingly, the time interval ( $\Delta t$ ) between two consecutive images is  $1/30$  seconds.

As mentioned in the beginning of this chapter, external factors, such as background noise or finger shaking, can easily and detrimentally affect the microscopic image. A sample of the original (raw) microscopic image is shown in Figure 3.8, with a size of  $480 \times 640$ . Apparently, poor contrast and resolution limit of the raw microscopic image make it very difficult to analyze. To deal with this issue, particular preprocessing strategy was designed to enhance the image quality before measuring the blood flow velocity. The strategy is described in Figure 3.9.

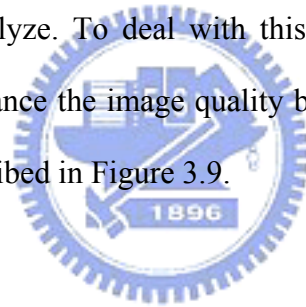


Figure 3.8 Original microscopic image of microcirculation.

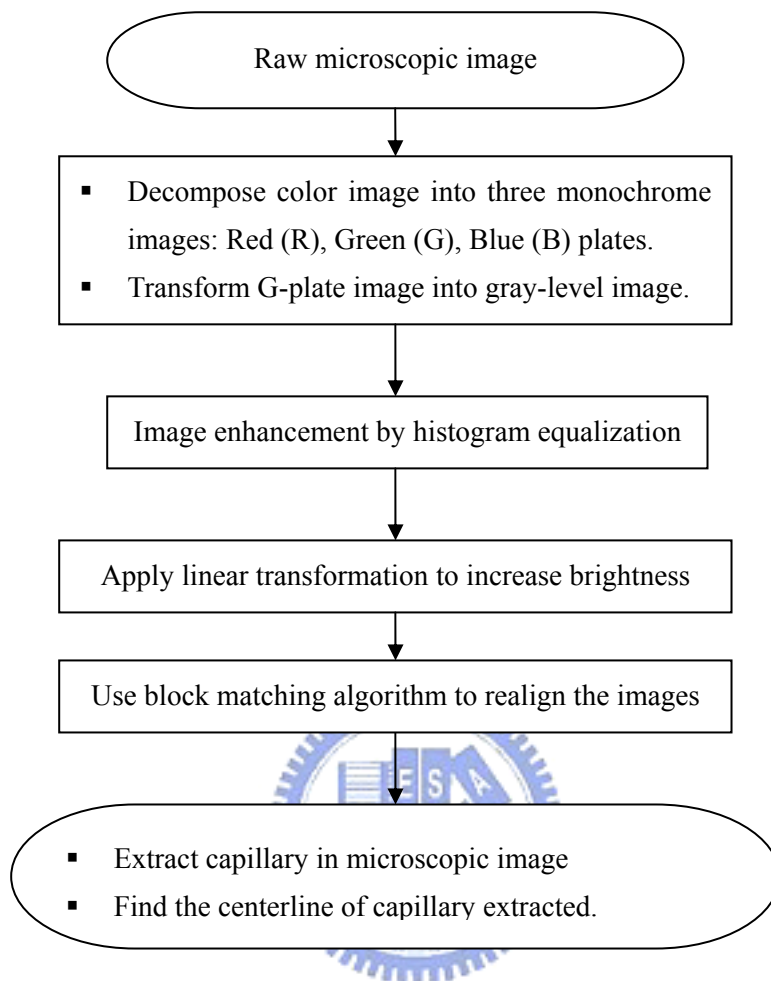


Figure 3.9 The strategy of preprocessing.

**Step 1:** Decompose the color image into three monochrome image (R-, G- and B-) plates. According to some literature [20], G-plate image reveals comparatively better quality for capillary microscopic investigation. Because of the red color of capillaries, we selected its complementary color, that is, the G-plate image. According to the theory of human vision fatigue, if someone looks at the red color for a while, the optic nerve will feel tired and will need a complementary color to recover from the fatigue.

However, a microscope with a green light source was not available with the instrument employed. The microscope applied in this study is installed with

white LED light. Therefore, the effect of a green light source was simulated by using the decomposed G-plate image. The original image and decomposed R-, G-, and B-plate images are presented in Figure 3.10.

Apparently, the R-plate image exhibits poor quality in contrast, while the G-plate and B-plate images provide clear descriptions. The detailed reason for choosing the G-plate image is to be discussed in Chapter 4.

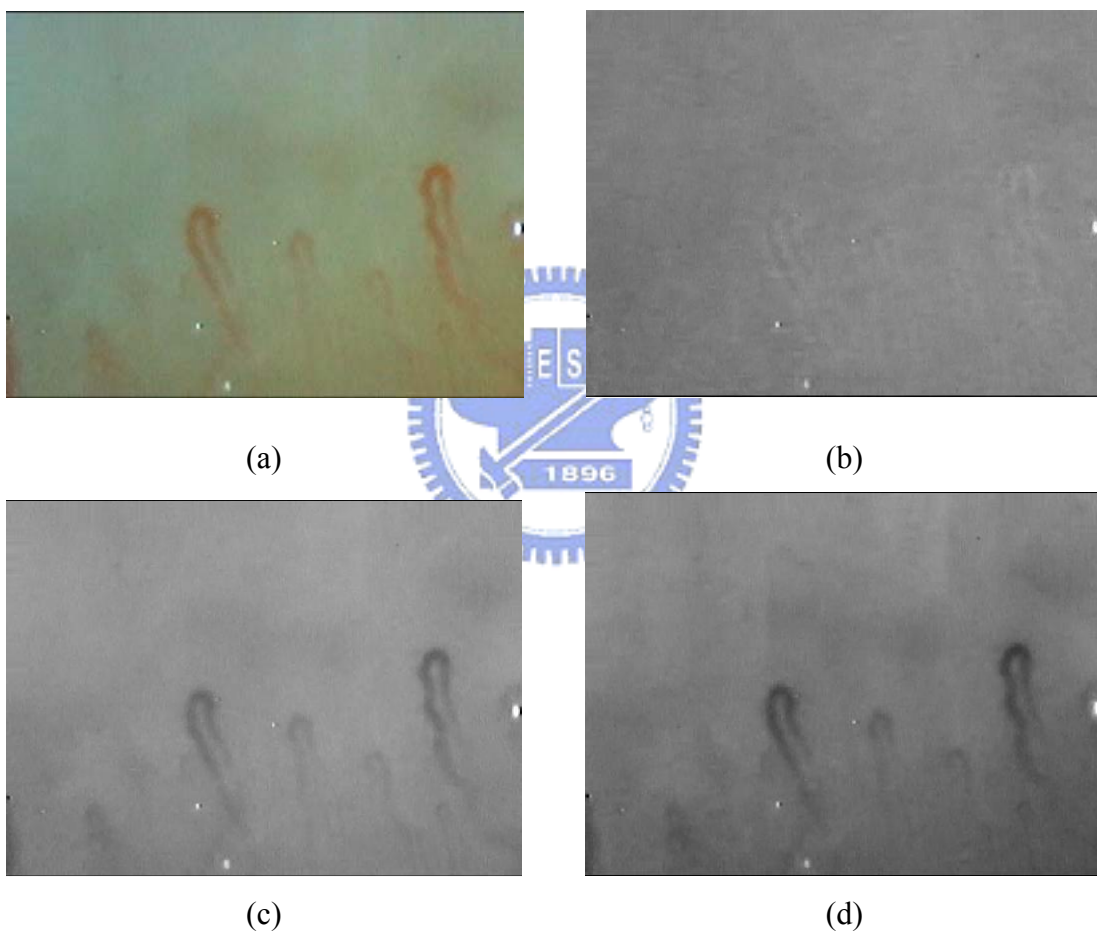


Figure 3.10 (a) Raw image, (b) R-plate image, (c) G-plate image, and (d) B-plate image.

**Step 2:** Histogram equalization for image enhancement was applied to the gray-level image to obtain a better contrast and clearer image of the capillaries. In

addition, this method also facilitates the observation of erythrocyte movement by naked-eye examination. Based on the probability theory, histogram equalization is a popular method for image enhancement.

**Step 3:** Gray-level transformation was applied to the image after histogram equalization. With careful selection of value of gamma, the image quality can be further improved that increases the accuracy of object (capillary) identification.

**Step 4:** Images extracted from various frames were realigned by using the block matching algorithm. Several images were grabbed during the experiment to deal with the issue of possible finger shaking. Details of realignment scheme are described in Section 3.4.

**Step 5:** Finally, a binary microscopic image of capillary was ready to be extracted from the realigned image. And a centerline of the extracted capillary was determined by image morphologic procedure – skeletonizing the binary capillary image. Section 3.5 depicts the approach in detail.

### **3.4 Dynamic Microscopic Images Realignment**

In this study, object alignment is a must for correctly identifying the blood capillary. We adopted block-matching algorithm [21] to do realignment. The block-matching algorithm is a standard technique for encoding motion in video sequences. It aims at detecting the motion between two images in block-wise sense. The blocks are usually defined by dividing the image frame into non-overlapping square parts. Each block from the current frame is matched into a block in the destination frame by shifting the current block over a predefined neighborhood of pixels in the destination frame. At

each shift, the sum of the differences between the gray values of the two blocks is computed. The shift that gives the smallest total difference is considered the best match. In this thesis, we used mean square difference (MSD) as matching criteria to compute the total difference between two blocks and executed full search in whole image. The MSD will be described in Section 3.4.2.

### 3.4.1 Block Matching Algorithm

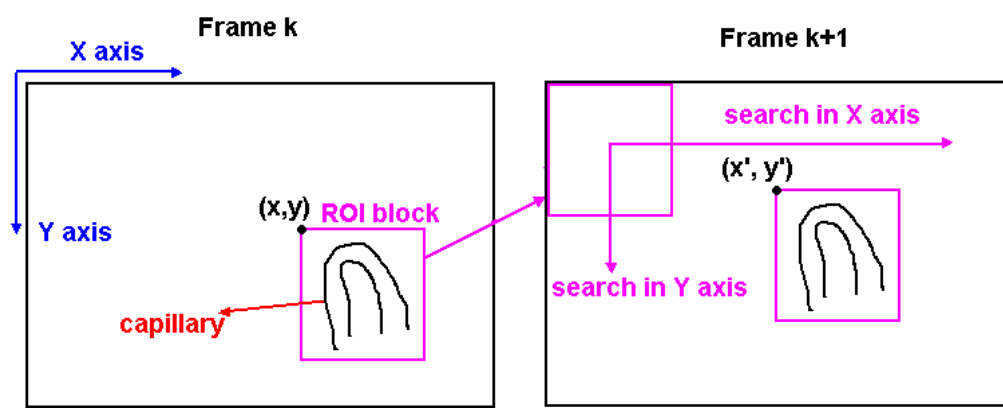


Figure 3.11 Illustration of block matching.

Feasibility of this method is based on two assumptions: 1) the images do not rotate, and 2) the images are not deformed.

We divided the image of frame k into several blocks with size  $128 \times 160$ . Next, we choose one block which contains most parts of a capillary as the region-of-interest (ROI) block. Then we use this ROI block as reference image to search for the same area in the image of k+1 frame by criteria MSD. We shift the ROI block with the step of one pixel along the X axis or Y axis each time, and derive the MSD value at each shift. Finally we will find the coordinate  $(x', y')$  corresponding to the smallest MSD value and then motion vector can be known for realignment.

### 3.4.2 Matching Criteria

There are four criteria with the advantage of computational efficiency and easy implementation: 1. Mean Square Difference (*MSD*), 2. Sum of Absolute Difference (*SAD*), 3. Cross-correlation Coefficient (*CC*), and 4. Standard deviation of gray-level ratio (*SDGR*). In this thesis, the *MSD* was applied as the criterion to identify the shifted images and was illustrated below. The other three criteria can be found in Appendix A.

#### *Mean Square Difference (MSD)*

The mean square difference (*MSD*) is similar to *SAD*, except that the gray-level difference is squared and the sum of squares is divided by the total number of effective pixels (*NEP*)

$$MSD = \frac{\sum_i \sum_j (S(i, j) - R(i, j))^2}{NEP} \quad (3.1)$$

We denoted the reference image as  $R(i, j)$  and the other image as  $S(i, j)$ , where  $i$  and  $j$  are the pixel coordinates of the image in the image space.

The block-matching algorithm was applied to two consecutive images. Once the shifting distance of the second image was known, it was then re-positioned in order to achieve a better match with the first (reference) image, also based on the *MSD* criterion. This process was repeated, for all the subsequent images, till each one achieved the optimal match with the reference image.

There are two matching schemes. The first involves matching all the images to the first image. The other scheme involves matching each image to the preceding one. According to Chen's thesis [11], the first scheme provides more accurate result. We thus adopted the first scheme and it will be discussed in detail in Chapter 4.

## 3.5 Segmentation and Skeletonization of Microscopic Capillary Images

### 3.5.1 Segmentation

After realignment, the desired segment (128×128 pixels, as shown in Figure 3.12(a)) was identified in order to get a binary microscopic capillary image. In this process of segmentation, Otsu's method [22, 23] was used to find the best threshold value for transforming the gray-level image into binary one. The image after segmentation is shown in Figure 3.12(b). The details of the Otsu's method can be found in Appendix B.

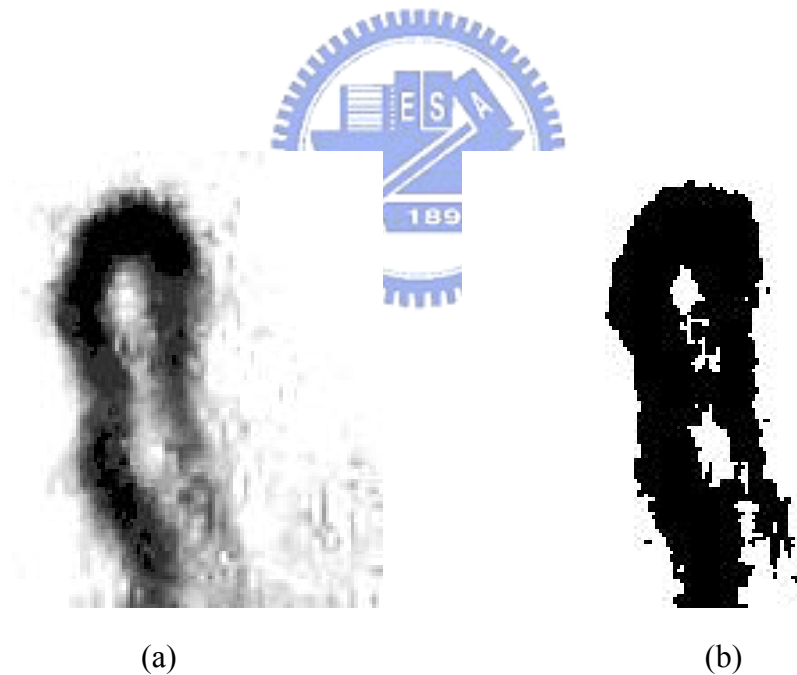


Figure 3.12 Capillary image (a) before segmentation (gray-scale image), and (b) after segmentation (binary image).

### 3.5.2 Skeletonization

Skeletonization is to determine the major pathway of blood flow. After the segmentation process, skeletonization can be applied to the binary capillary image. In this study, Zhang-Suen skeleton algorithm [24] was adopted for skeletonization because of its advantages of easy implementation and computational efficiency. The resulting image, blood-flow pathway, provides a reliable estimate for capillary blood velocity. The images before and after skeletonization using the Zhang-Suen algorithm are presented in Figure 3.13. Based on the skeletonized image in Figure 3.13(b), we selected the middle section for estimating blood-flow velocity. The top and bottom sections involve curves that may make the estimate difficult and unreliable. Details are discussed in Chapter 4.

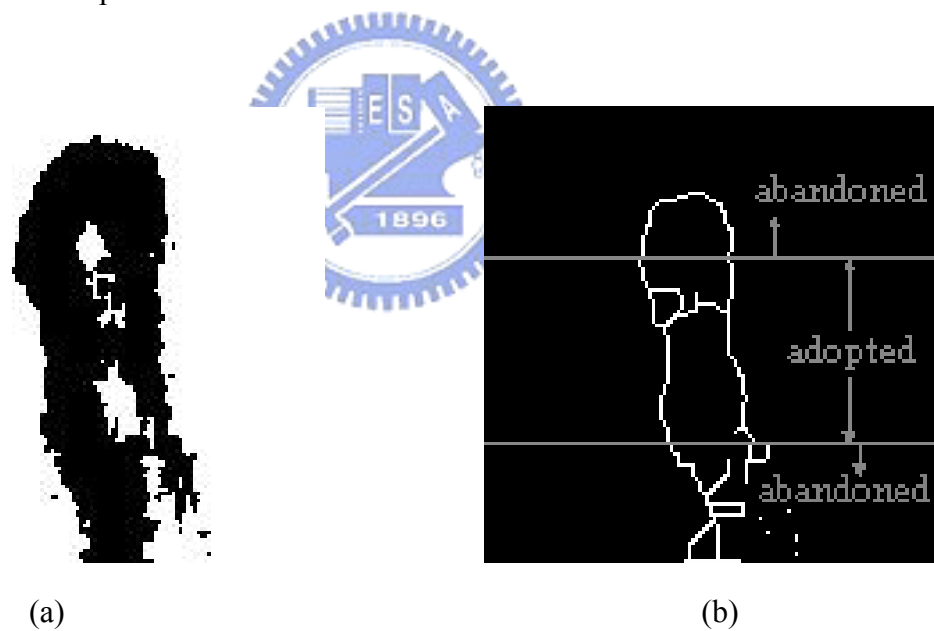


Figure 3.13 (a) Binary capillary image before skeletonization, and (b) blood-flow pathway derived by skeletonization.



### 3.6 Procedure of Estimating Capillary Blood Velocity

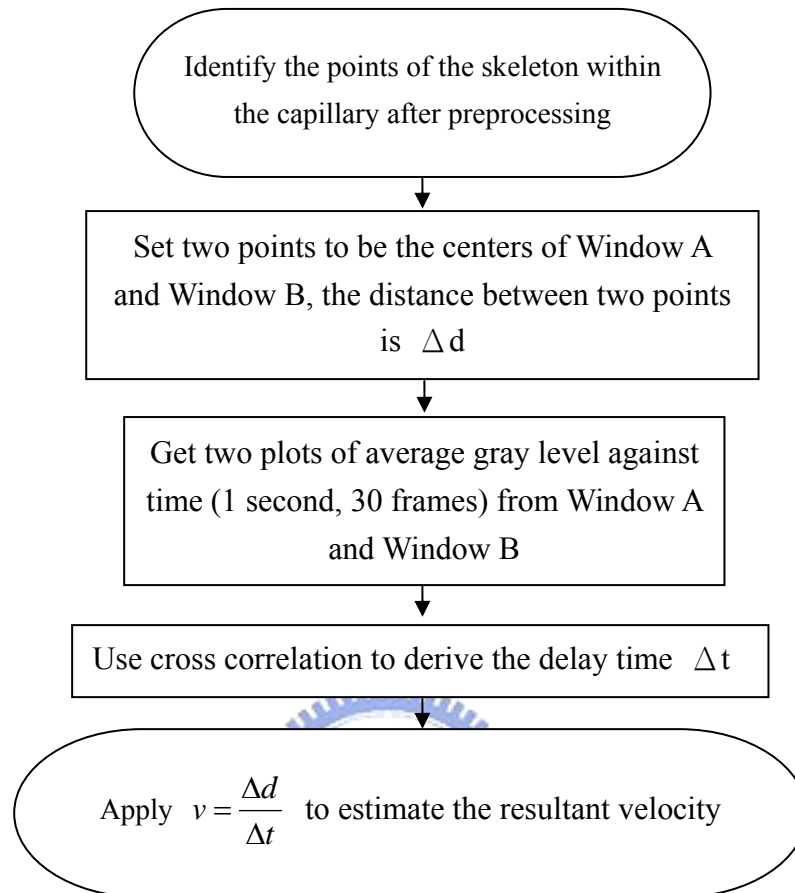


Figure 3.14 Procedure of estimating CBV by dual-windows method.

- Step 1. First, the useful points (the points of the skeleton within the capillary) locating at the left side of the capillary skeleton (Figure 3.13(b)) need to be identified.
- Step 2. From these points, we select two points to be the centers of Window A and Window B manually. Besides, according to the conclusion by Tsukada in Section 2.2.1, we define the Window A and B to be circular windows and the diameter of each window is 5 pixels= $7.6 \mu\text{m}$  in this study in order to increase the accuracy. Therefore the coordinates of the centers are determined, as shown in Figure 3.15, Notice that the blood cell flows through Window A first.



Figure 3.15 A diagram of the two chosen windows.

Step 3. 30 frames (images) are inspected. In other words, average gray levels of both Window A and Window B were observed for the duration of one second (30 frames /sec). Figure 3.16 presents the graph of the average gray levels varying with time (frame)

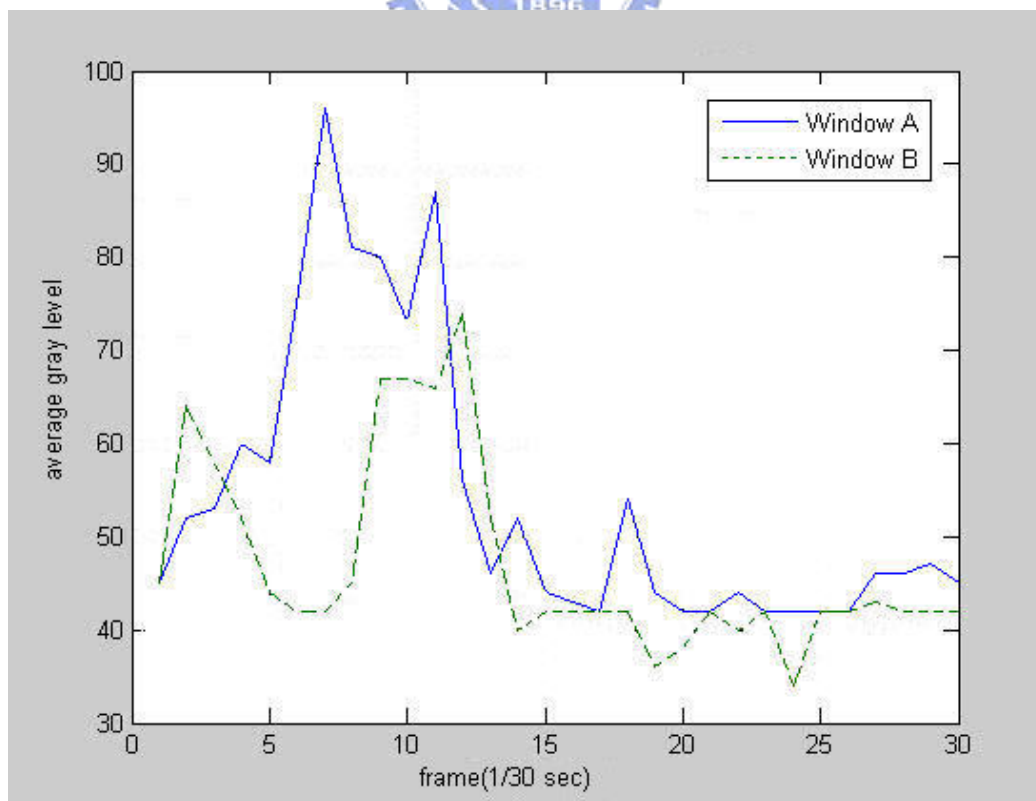


Figure 3.16 Average gray level plotted against time.

Step 4. In order to derive the time difference  $\Delta t$  automatically in Figure 3.16, cross-correlation method was applied [13]. The equation of cross-correlation is:

$$R_{xy}(m) = \sum_{n=0}^{N-m-1} x_{n+m} y_n^*, \quad m = 1, 2, \dots, 2N - 1 \quad (3.2)$$

where  $N$  is the length of  $x$  and  $y$  ( $N=30$  in this study; it represents 30 frames), and  $m$  is the shift in points (one point equals to one frame, i.e. 1/30 seconds in time). Examine out the index  $m$  of maximum value of  $R_{xy}(m)$ , then the time difference  $\Delta t$  that a specific blood cell move from Window A to Window B can be derived.

Step 5. Finally, the capillary blood velocity was estimated by  $v = \frac{\Delta d}{\Delta t}$ .



# Chapter 4

## Results

In the first section of this chapter, we discuss the effect of instrument setting and demonstrate that the G-plate component is the best choice for further analysis. In regard to the instrument setting, we show that different positions of LED light source result in various image qualities. The reason of selecting G-plate component is illustrated by histogram profiles. Section 4.2.1 discusses two different schemes for realignment and the resulting performance. Section 4.2.2 states the condition in which the MSD algorithm fails. Section 4.3 presents the morphological approach and three rules for locating the centers of two observation windows. In section 4.4, we first establish a reference value of velocity by naked-eye examination. Then, the precision of proposed scheme is demonstrated by the average and standard deviation of 100 estimates. Finally, we will present the results of analyzing the data acquired from four subjects, including two Zen-meditation practitioners and two normal, healthy subjects in the same age range, yet without any meditation experience.

### 4.1 Effects of Instrumentation Setting on Image Quality

A number of factors affect the resulting quality of capillary image. First of all, the appropriate instrumentation setting is important for acquiring images with good quality. As mentioned in Section 3.3, the beginning step is to determine the appropriate position of LED light on the microscope. The schematic diagrams below (Figure 4.1) demonstrate two possible positions, that is, the LED light source emitting

either from the upper back or from the upper front of the finger.

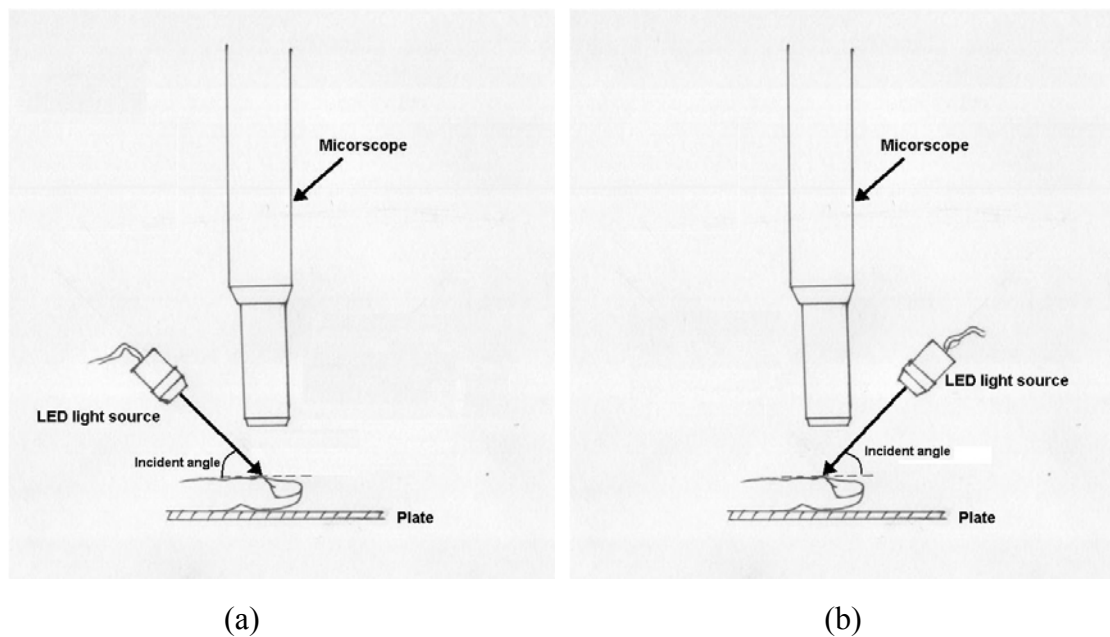


Figure 4.1 Schematic illustration for illumination source from (a) upper back, and (b) upper front of the finger.

According to a book, “Microcirculation Methodology [8]”, the illumination from the upper front of the finger (Figure 4.1(b)) would produce a microscopic image with clearer capillary contours. We thus conducted a preliminary, empirical test. Figure 4.2 displays the images recorded. According to naked-eye examination, the image recorded with illumination from the upper front (Figure 4.2(b)) apparently reveals clearer profile for the capillaries.

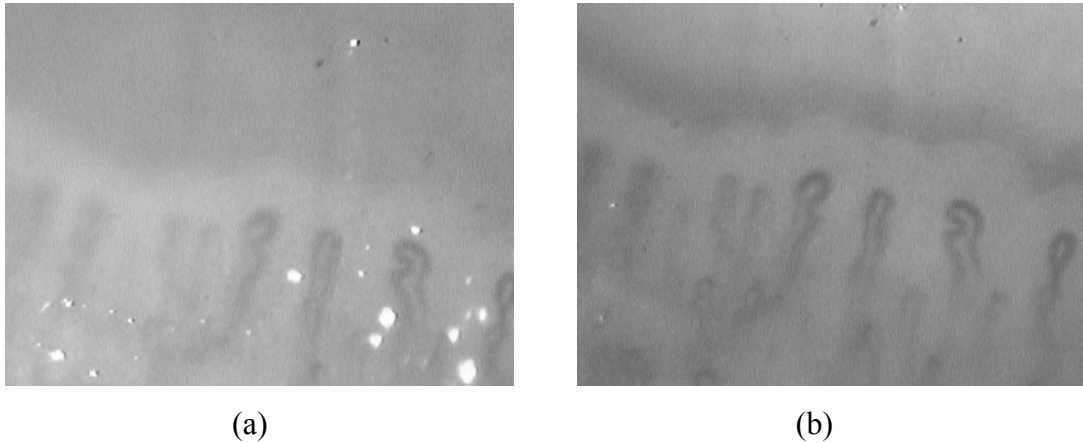


Figure 4.2 Images acquired by illumination locating at (a) upper back, and (b) upper front of the finger.

The second factor deals with the selection of decomposed monochrome plate. The image analysis method developed is applied to the gray-scale image. Direct transformation of the original RGB image into gray-scale one often results in contours with low contrast due to complex tissues photosensitizing the red, green, or blue color at various levels. To solve this problem, the original RGB color image needs to be decomposed into three monochrome plates first, from which we further identify the one providing the best contour profile for capillaries. The resultant monochrome images and their corresponding histograms are presented below (Figure 4.3).

From the illustration in Figure 4.3, the red-plate image exhibits poor contrast and blurred edges that can be further corroborated from the narrow, mid-tone distribution of the histogram of R-plate image. It is due to the color similarity between R-plate image and the color of object of interest (capillary). Comparing the histograms between G-plate and B-plate image, the later has a wider range of gray-scale levels, indicating a better contrast. However, in [20], the author claimed but did not attempt to prove that B-plate image had more noise than the G-plate image. In this thesis, we aimed to demonstrate scientific evidence based on their histograms.

We first identified two  $128 \times 128$  white square regions, in Figures 4.3(c) and 4.3(e), containing the selected capillaries. The windowed segments shown Figure 4.4 are magnified for better visual aid. Their corresponding histograms are plotted in Figure 4.5(a) and (b).

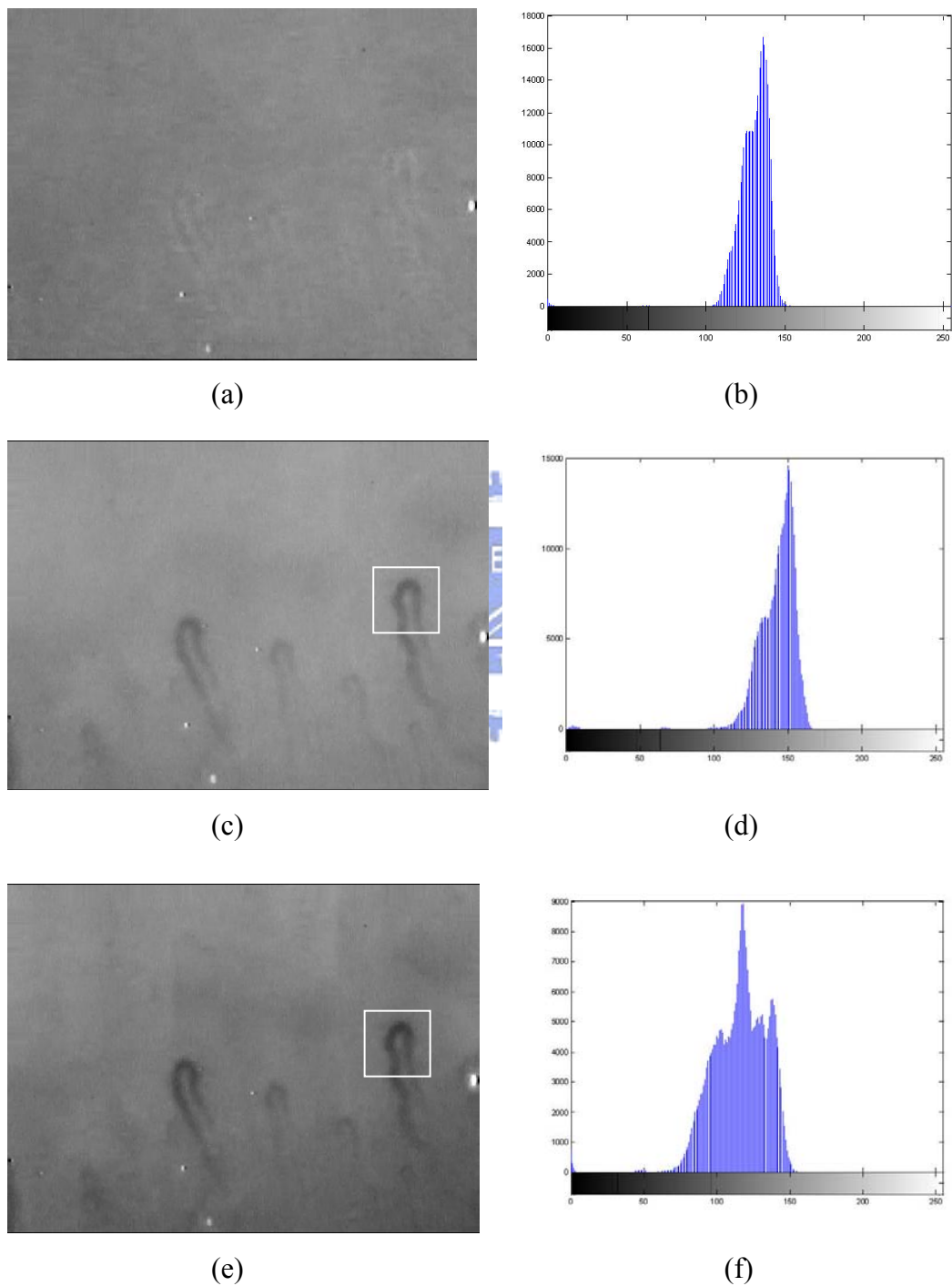


Figure 4.3(a) R-plate, (b) histogram of R-plate image, (c) G-plate, (d) histogram of G-plate, (e) B-plate, and (f) histogram of B-plate.



Figure 4.4 White-squared segment of (a) G-plate image, and (b) B-plate image in Figures 4.3(c) and 4.3(e), respectively.

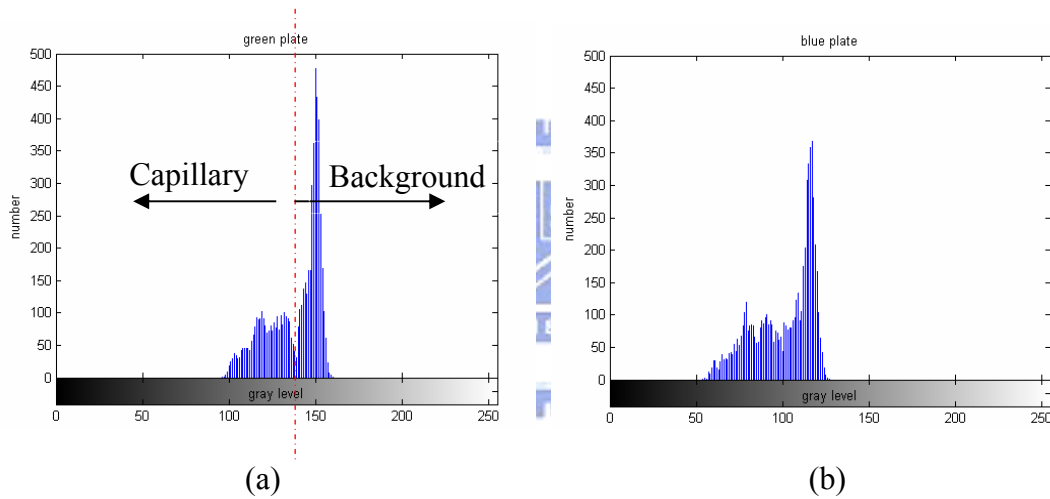


Figure 4.5 Histogram of (a) Figure 4.4(a), and (b) Figure 4.4(b).

According to the histogram distribution of Figure 4.5(a), we may identify two separable gray-level regions divided by the gray value of approximate 140, as indicated by the dashed line.

We analyzed the histograms of local blocks selected from either clean background or complete capillary regions, without overlapping each other, to investigate their regions of histogram focalization. The results (Figure 4.6) demonstrate that the section to the left of the dashed line ( $<140$ ) corresponds to the gray-level distribution



of the capillary, while the other section with gray levels larger than 140 represents the gray-level distribution of the background (Figure 4.6(a)). However, the B-plate histogram in Figure 4.5(b) cannot be firmly divided into two sections due to the absence of a similar dip. As a result, the G-plate component provides the useful information of determining the parameter required by image segmentation and feature extraction.

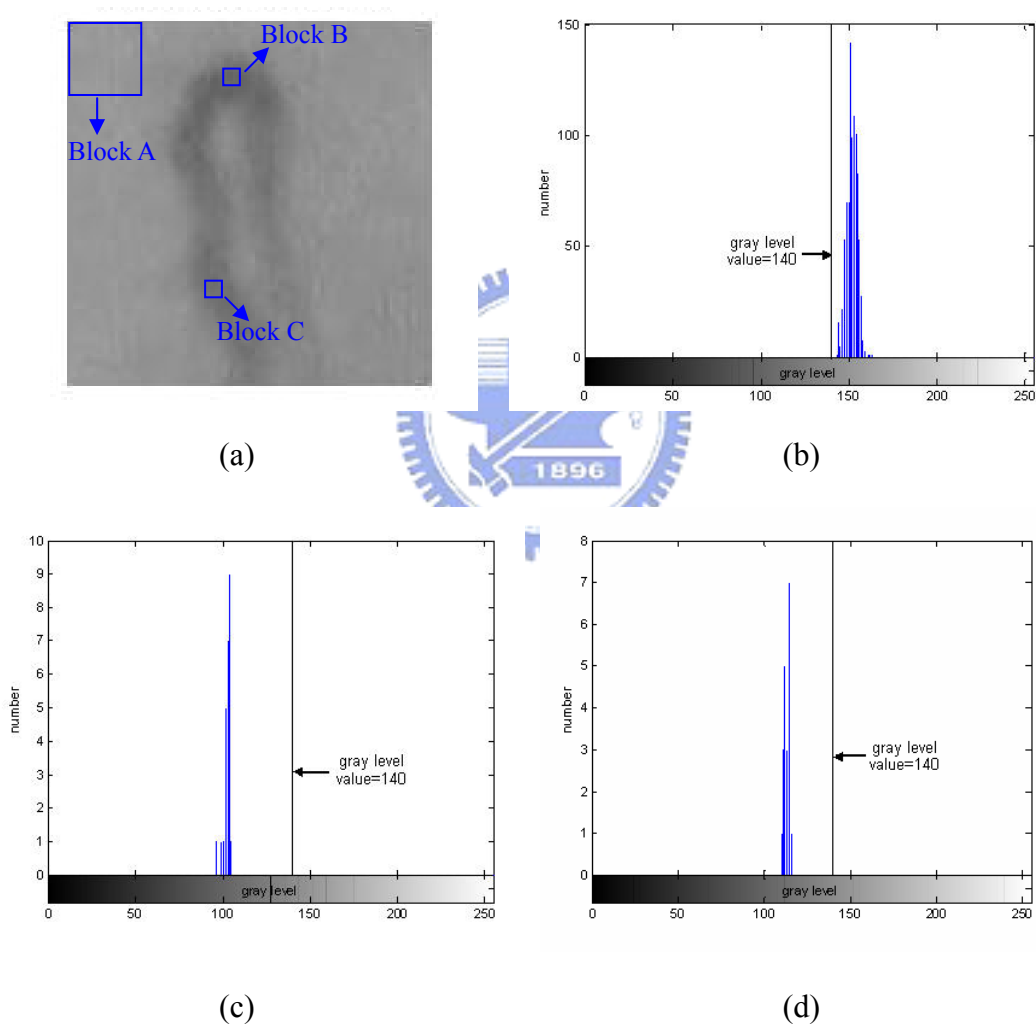


Figure 4.6 (a) G-plate image, (b) histogram of block A (background, size: 30×30), (c) histogram of block B (capillary, size: 5×5), and (d) histogram of block C (capillary, size: 5×5).

In Figure 4.7, the binary images obtained by Otsu's method reveal the advantage of employing the G-plate component at the segmentation stage of preprocessing.

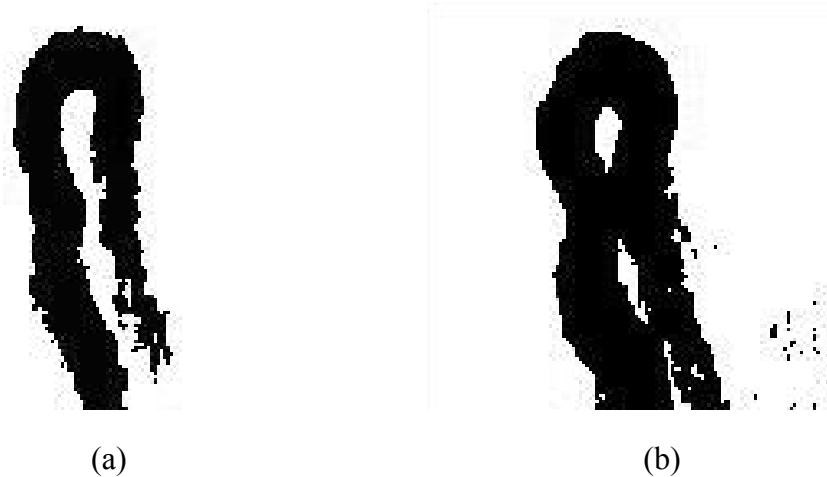


Figure 4.7 Binary images derived from (a) G-plate component, and (b) B-plate component.

As shown in Figure 4.7(b), the right-loop capillary severely merges with the left loop that results in indistinguishable contours of the capillary walls. Moreover, there are many spots and blotches outside the capillary. Such adverse effects on the binary image will lead to poor performance in skeletonization. According to the above demonstration by Figures 4.6 and Figure 4.7, the G-plate component is evidently the optimal choice for the purpose in this thesis.

## 4.2 Issue of Realignment

### 4.2.1 Comparison Between Two Methods for Realignment

To realign the shifted microscopic images, Section 2.4 introduced two methods: 1) matching all the subsequent image frames to the first frame, and 2) matching each

frame to the preceding one. The following illustration provides the evidence that the first method is better than the second one.

To compare the performance of both realignment methods, we first simulated nine shifted microscopic images with known steps of shift and one without shifted as the original image. The original image and shifted image (shifted downward) of size  $640 \times 480$  are plotted in Figure 4.8. Note that the vacant region of the shifted image was filled with black (gray level = 0). As shown in Figure 4.8(b), the upper region was painted with black color when the image shifted downward.

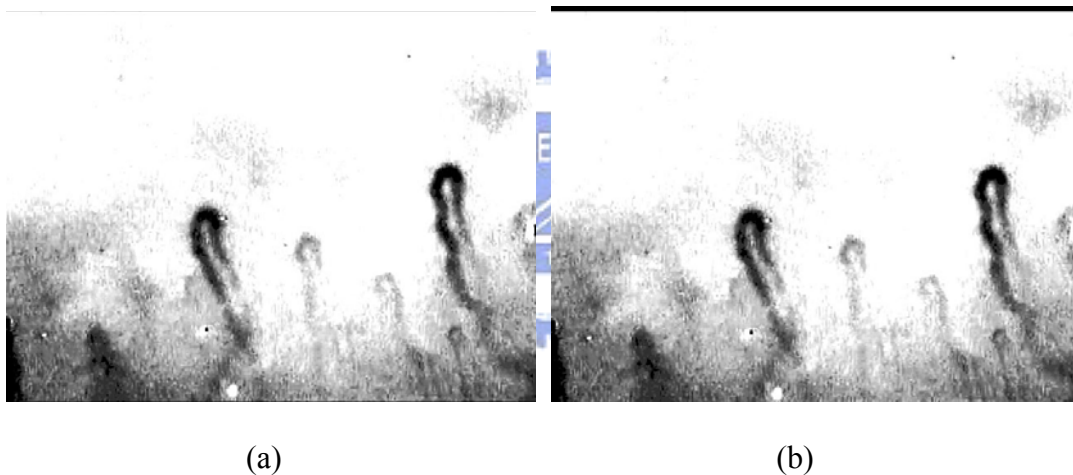
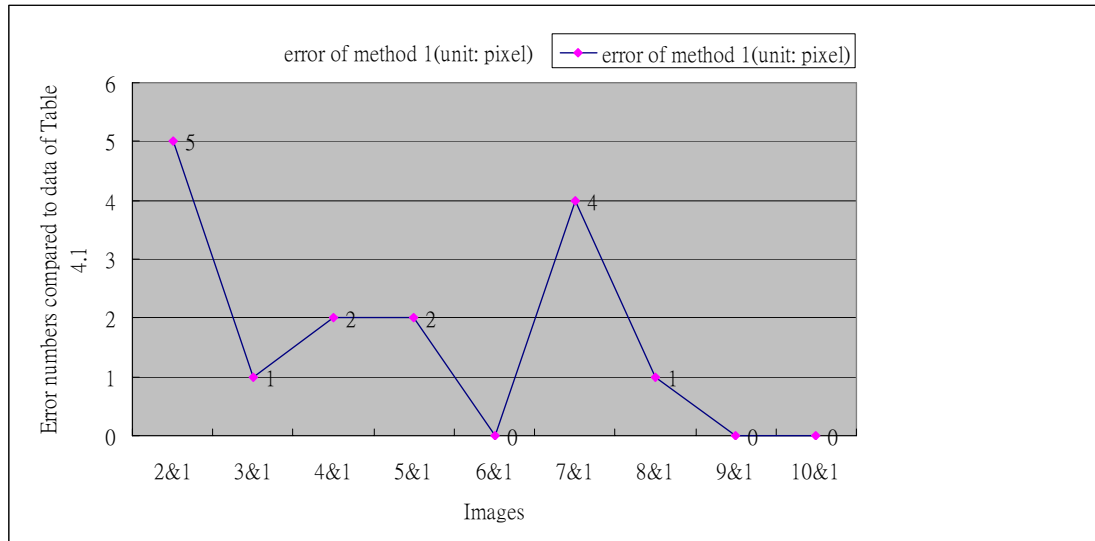


Figure 4.8 (a) Original image, and (b) shifted image (shifted downward).

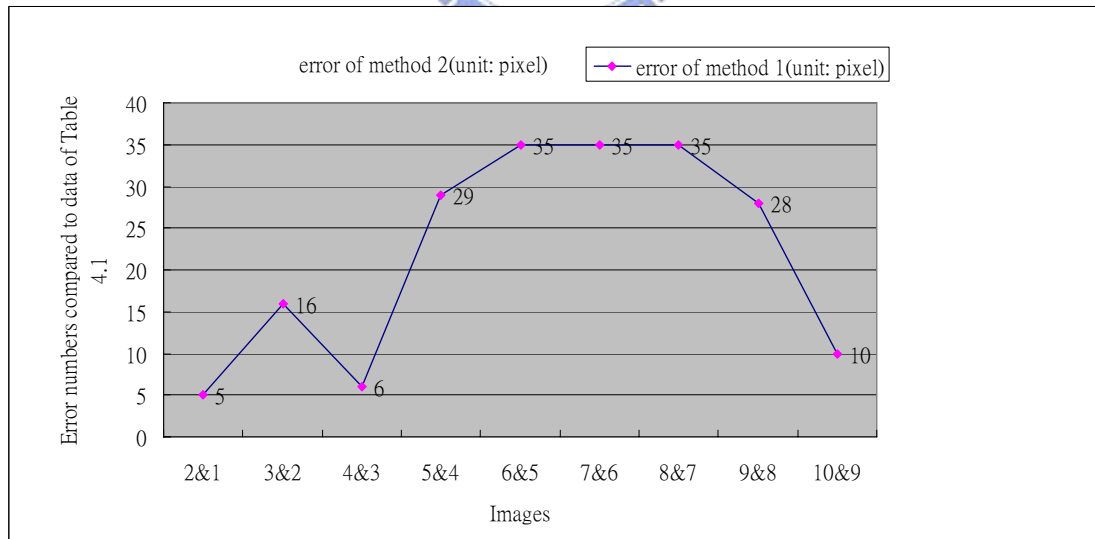
Table 4.1 lists the number of shifted pixels along each coordinate. Following equation (2.2), we obtained the errors in image realignment based on Method 1 (Figure 4.9 (a)) and Method 2 (Figure 4.9 (b)).

Table 4.1 Number of shifted pixels used to generate ten shifting images.

Image index	1	2	3	4	5	6	7	8	9	10
Horizontal (+: rightward)	0	-5	0	0	9	-9	9	-9	10	-10
Vertical (+: upward)	0	0	-6	6	-8	-8	8	8	0	0



(a)



(b)

Figure 4.9 (a) Error in realignment using Method 1, and (b) error in realignment using Method 2

The horizontal coordinates in Figure 4.9 represent the indexes of the image pair for realignment. Evidently, errors resulted from Method 2 are significantly larger than those resulted from Method 1. Therefore, the first method is applied for image realignment.

#### 4.2.2 A Greater Error in Realignment

Inappropriate preprocessing of the microscopic image may cause a larger error in the realignment. Figure 4.10 displays the images without proper preprocessing.

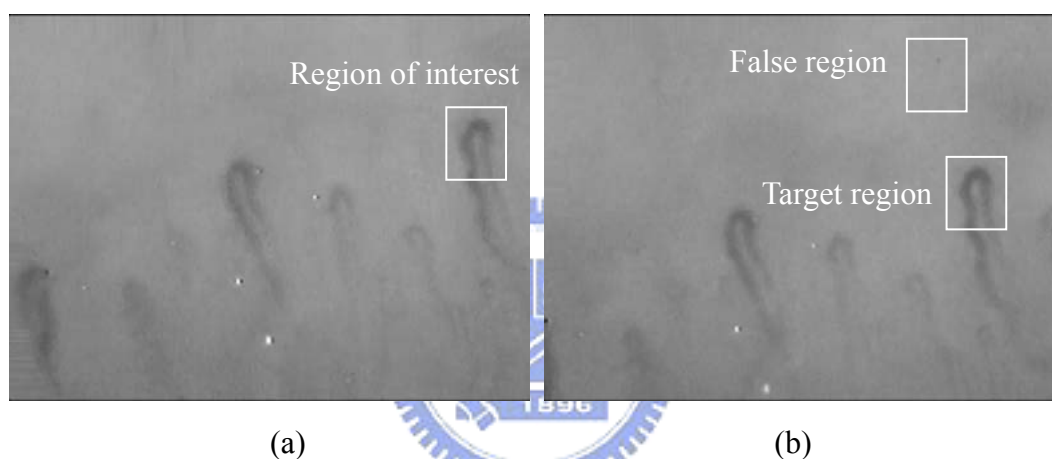


Figure 4.10 Image frames selected from the same video: (a) the 1491<sup>st</sup> frame, and (b) the 1<sup>st</sup> frame.

Based on the block matching algorithm, the procedure for realigning these two images is to choose a region of interest (ROI) in Figure 4.10(a) (size: 128×160 pixels) and to find a target region of the same size. The target region is validated by the minimum MSD compared with ROI. An appropriate block matching process allows one to find the corresponding target region in Figure 4.10(b) and, according, determine the number of shifted pixels. However, it may happen that the area with the smallest MSD is not the desired target region (Figure 4.10(b)). The MSD values computed for the example shown in Figure 4.10 are 1,490 and 22,804 for the false region and the target region, respectively.

The example above demonstrates the situation that block matching algorithm failed to find the correct target region due to the improper preprocessing. This problem can be solved by an appropriate preprocessing step that enhances the contrast between the capillary and its background.

### 4.3 Morphological Approach for Locating Observation Windows

Locations of two observation windows play an important role in reliable estimate of blood flow velocity. Ideally, the observation window should be positioned on the pathway of blood-cell flow. To ensure the correct location, we applied the skeleton method to restrict the searching region to the capillary. Figure 4.11 illustrates an example. By checking the gradients, points A and B are located approximately at the edge of the capillary. The distance between A and B (marked by two white dots) can be considered as the capillary diameter which is 18 pixels ( $27.36 \mu\text{m}$ ) in this case Figure 4.11(c)). As the diameter of observation window is 5 pixels, the range of observation window located by skeletonization is apparently within the capillary canal. Accordingly, the window can be ensured to cover the blood-cell pathway so that we may reliably capture the blood cell flow.

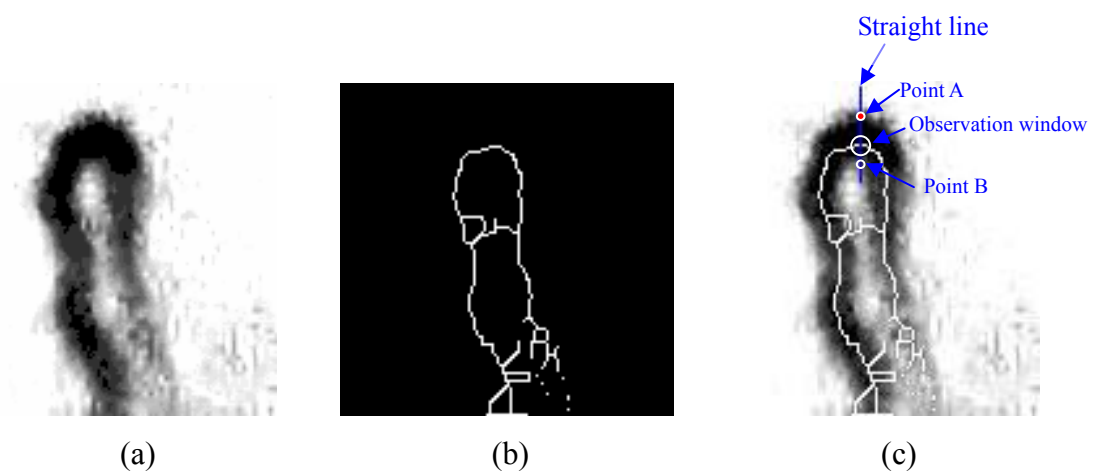


Figure 4.11 (a) Original image, (b) skeleton image, and (c) overlapping image.

The rules listed below need to be applied when choosing the center points of the dual-windows.

1. Choose two points from the straight-line segment of the skeleton; otherwise, the passage causes more resistance to the blood cells.
2. Avoid choosing the points on the upper curve of the skeleton where the estimate tends to be unreliable.
3. Avoid choosing two points which are close to each other. Note that the accuracy of the dual-windows method depends on the variation of gray-level values within two observation windows. The in-between distance cannot be smaller than the diameter of a blood cell, otherwise, the estimate may be difficult and unreliable (Figure 4.12). In general, the diameter of a blood cell in the capillary is approximately  $5-7\mu m$ . Therefore, the distance between two observation windows needs to be at least  $7\mu m$ .

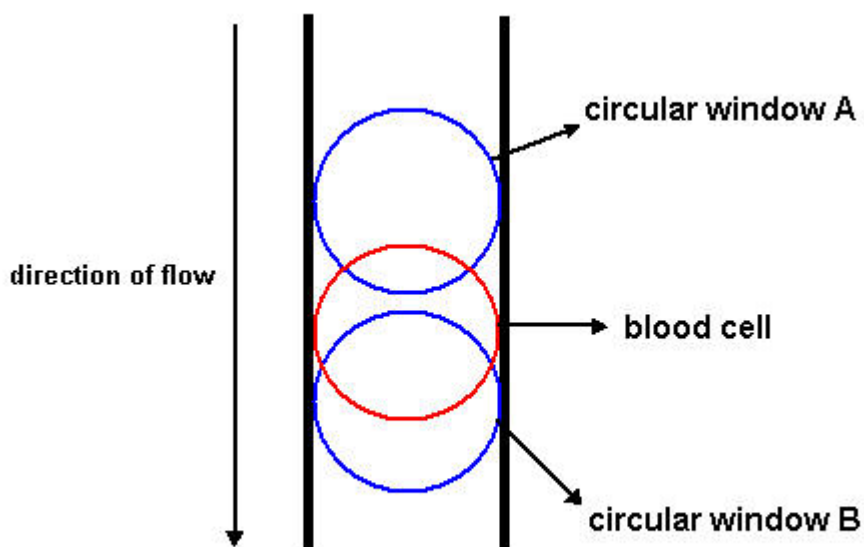


Figure 4.12 Illustration of insufficient distance between two observation windows.

## 4.4 Estimation of Capillary Blood Velocity

As a reference, we first observed the movement of blood cell by checking the coordinates of two observation windows. This would be considered as the reference velocity. Next, we adopted the proposed algorithm and strategy to execute 100 estimates of capillary blood velocity from 100 non-overlapping microscopic image sets. We assume the capillary circulatory system is steady in the sense that blood flows at an approximately constant rate within a time period of one minutes. From the distribution of 100 velocity-estimate samples, we computed the mean value and standard deviation to demonstrate the reliability of the proposed scheme.

### 4.4.1 Estimate of Capillary Blood Velocity by Finding the Center of Blood Cell

In order to obtain a reference of capillary blood velocity beyond the computerized approach, we first estimated the velocity manually by finding the coordinates of center points of windows via MATLAB. Using MATLAB, we can create a smallest circle capable of containing most pixels of the blood cell (Figure 4.13). The center of the smallest circle thus can be considered as the center of the blood cell.

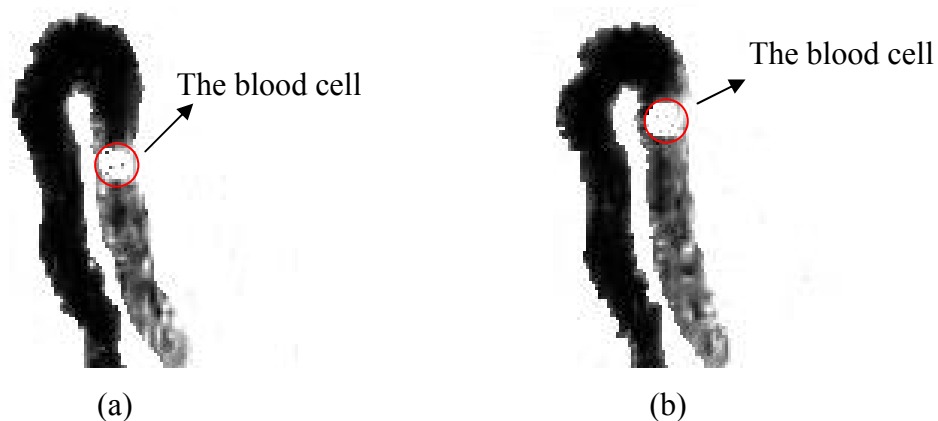


Figure 4.13 Capillary image of (a) the 167<sup>th</sup> frame, and (b) the 168<sup>th</sup> frame.



The 167<sup>th</sup> frame preceded the 168<sup>th</sup> frame by  $\Delta t=1/30$  second. By determining the coordinates of the center of the aimed circle in each frame, we can compute the distance  $\Delta d$  between two centers, which is  $23.52\mu\text{m}$  (16 pixels). Finally, the estimated capillary blood velocity is  $705.6 \mu\text{m}/\text{sec}$  according to  $v = \frac{\Delta d}{\Delta t}$ , which is used as the reference value for later comparison.

#### **4.4.2 Estimate of Capillary Blood Velocity by Proposed Scheme**

This section presents the results of estimating the capillary blood velocity using the proposed scheme mainly based on the dual-windows method. Totally thirty frames were analyzed in one estimate. Besides, we initially designated the center of Window A (B) to be the skeletal point as shown in Figure 4.14(a). Then we doubled the in-between distance by moving Window A downwards (Figure 4.14(b)).

After computation by our proposed scheme, the delay time in Figure 4.14(a) and Figure 4.14(b) are  $1/30$  second and  $2/30$  second, respectively.

Here we use the proposed scheme to estimate the velocities using different window position shown in Figure 4.14(a) and (b). The resultant velocities based on the two windows are the same:  $v=729.6 \mu\text{m}/\text{sec}$ . The results implied that the velocities of the blood cells in the straight line are almost the same, and that might eliminate the misgivings of the positions of the windows. Figure 4.15(a) and (b) provide plots of the gray-level variations during one second (30 frames) resulted from different distance of two observation windows.

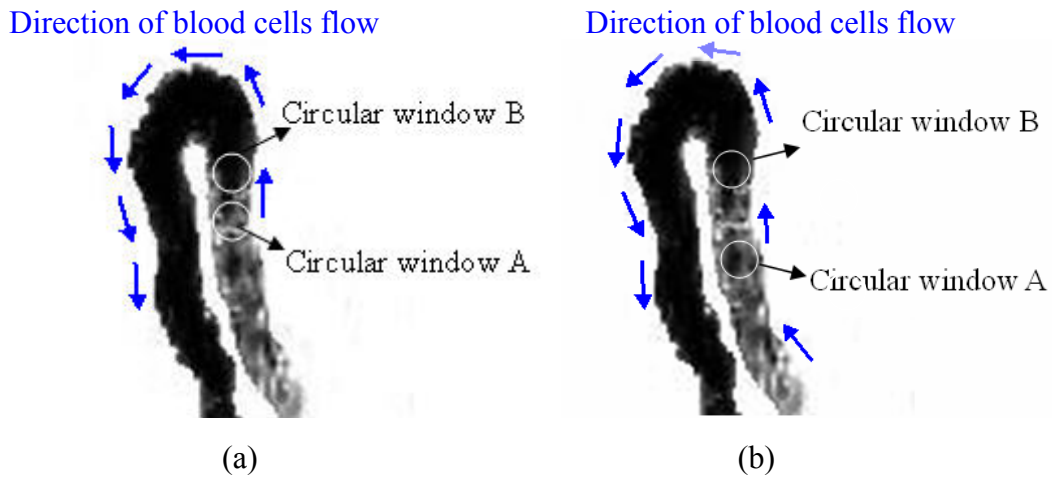


Figure 4.14 (a) Initial positions of two windows, and (b) desired positions of two windows with Window A descending.

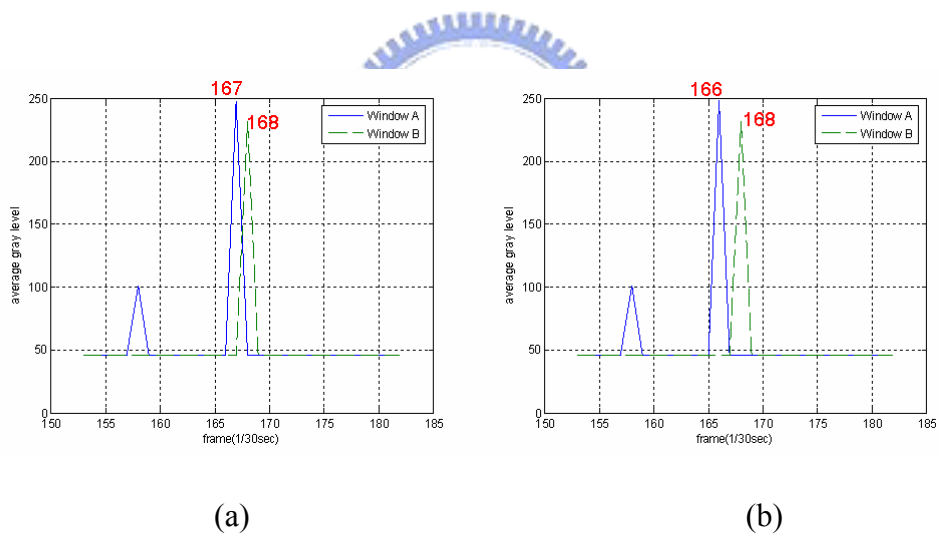


Figure 4.15 The one second, gray-level variations inside Window A and Window B using (a) the initial window positions, and (b) the modified window positions with double in-between distance.

Next, we estimate the capillary blood velocity for 100 non-overlapping, frame sets. The results are listed in Table 4.2 and plotted in Figure 4.16. The average velocity of 100 estimates is  $1029.3\mu\text{m}/\text{sec}$  with standard deviation  $208.64\mu\text{m}/\text{sec}$ . We can see that phenomenon of fluctuations reveal in each resultant velocities plot. According to M. Hahn's study [25], he measured the capillary pressure and capillary blood velocity (CBV) of normal people simultaneously in his experiment. The results reveal that the amplitude of the capillary blood pressure and CBV showed strong correlation. The author suggested that the pressure gradient across the capillary loop, which is the driving force for CBV, was mainly dependent on precapillary resistance. The regulation mechanism of blood flow in capillaries was also discussed in [26]. Moreover, Phillip [27] showed the flow equation below could be suitable for small Reynolds number



$$Q = \frac{\pi R^4}{8L\eta} \Delta P, \text{ where} \quad (4.1)$$

$Q$ : flow rate,

$L$ : length of an ideal tube,

$R$ : radius of an ideal tube

$\Delta P$ : pressure difference between the two extremities of the tube

$\eta$  : viscosity of fluid

Note that the radius ( $R$ ) and the cross-section area of capillary are almost constant. Therefore, for a fixed length ( $L$ ), the blood flow depends on the viscosity ( $\eta$ ) and the difference of pressure ( $\Delta P$ ). The  $\Delta P$  depends on the vasomotion of arterial smooth muscle and precapillary sphincters. According to Carr and Lacoïn's study [28], the viscosity depends on Fåhræus effect and it is also the cause resulting in the fluctuation of blood flow.

According to the above references, we suggest that the fluctuation of CBV is mainly related to the vasomotion and the non-uniform distribution of the blood cells.

Table 4.2 The 100 estimates for capillary blood velocity based on 100 non-overlapping frame sets.

1470	913	731	1162	974	729	867	958	958	825
1109	822	958	867	825	1284	822	974	974	822
974	822	1095	1140	1284	822	822	867	1148	822
1004	958	822	1004	1420	1374	1095	731	958	1095
825	1297	731	913	1162	958	958	1162	1004	1334
958	1095	1140	1004	1049	825	1374	958	822	825
867	974	825	1420	1109	1004	822	1420	1140	1284
1095	822	1606	1297	1297	1420	1095	1095	1109	1297
1049	974	1334	1561	1297	974	867	731	780	958
1297	731	958	867	1004	822	1140	974	1049	822

Unit: ( $\mu$  m/sec )

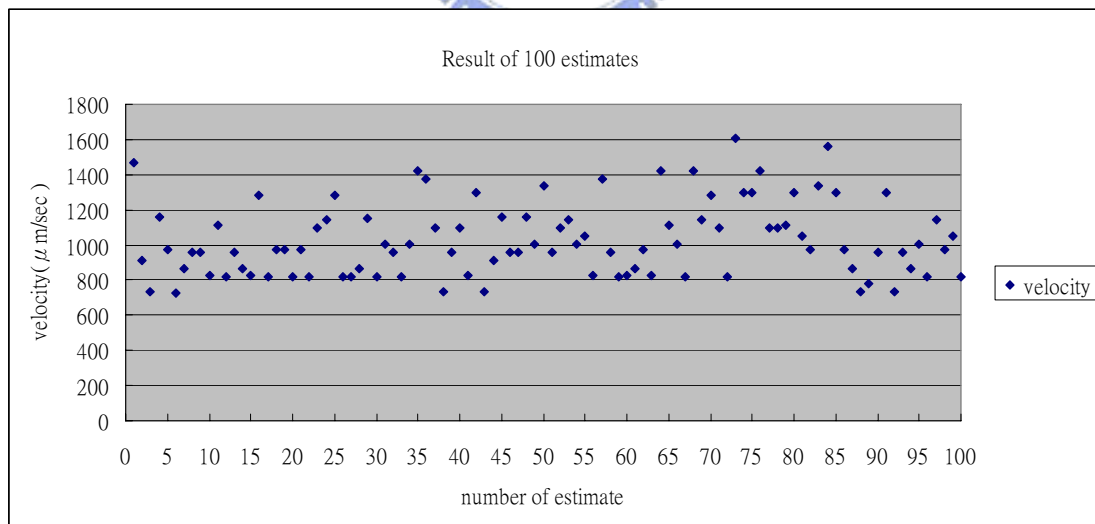


Figure 4.16 The 100 estimates for capillary blood velocity based on 100 non-overlapping frame sets.

Finally, we compared the results of analyzing one-minute capillary blood-flow velocities for four subjects, including two meditation practitioners (experimental subjects) and two normal, healthy subjects without any meditation experience (control subjects). They were about the same age. Figures 4.17 and 4.18 display the results of two experimental subjects. The average velocity of 60 estimates is  $995.4 \pm 186.1 \mu\text{m}/\text{sec}$  and  $1046.7 \pm 187.4 \mu\text{m}/\text{sec}$ , respectively.

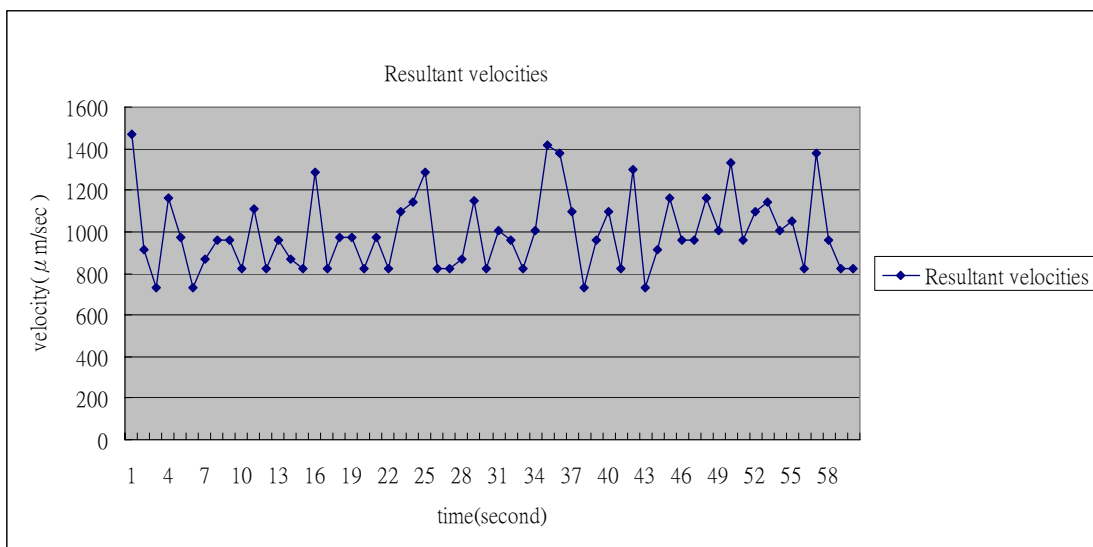


Figure 4.17 Estimate of one-minute capillary blood velocity for experimental subject 1.

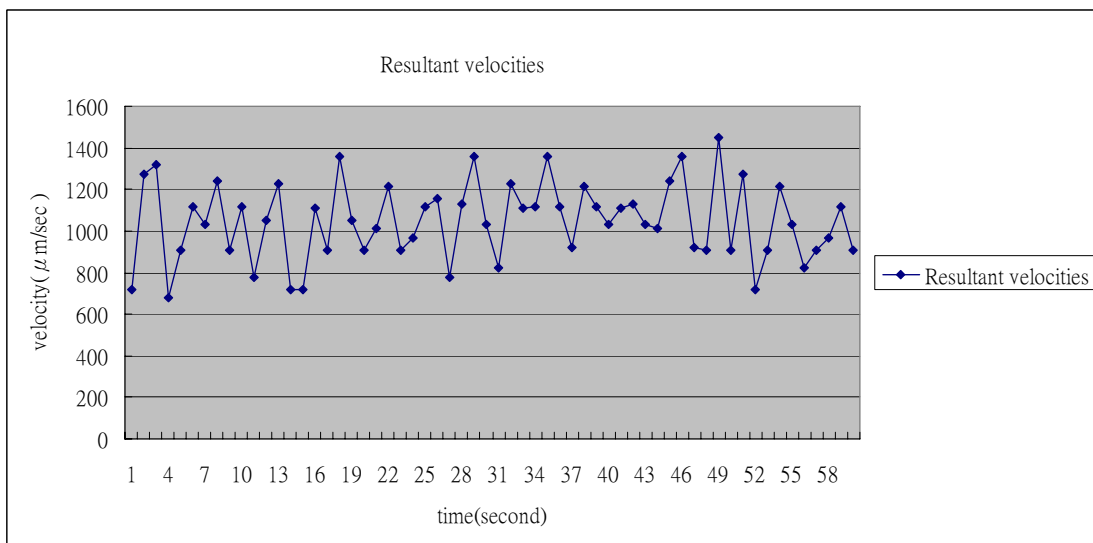


Figure 4.18 Estimate of one-minute capillary blood velocity for experimental subject 2.

Figures 4.19 and 4.20 display the results of two control subjects. The average velocity of 60 estimates is  $451.1 \pm 112.9 \mu\text{m}/\text{sec}$  and  $591.1 \pm 121.0 \mu\text{m}/\text{sec}$ , respectively.

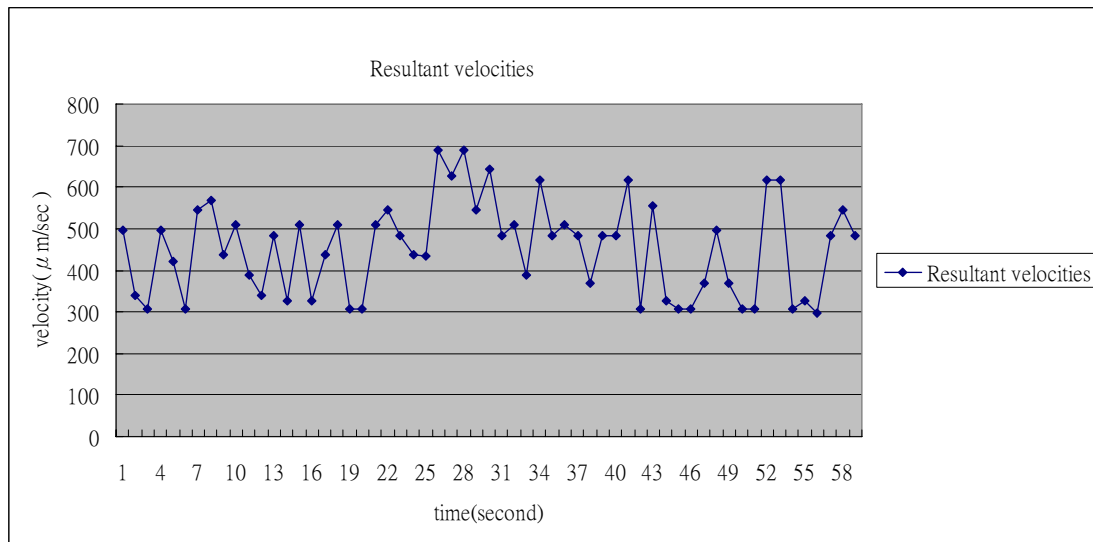


Figure 4.19 Estimate of one-minute capillary blood velocity for control subject 1.

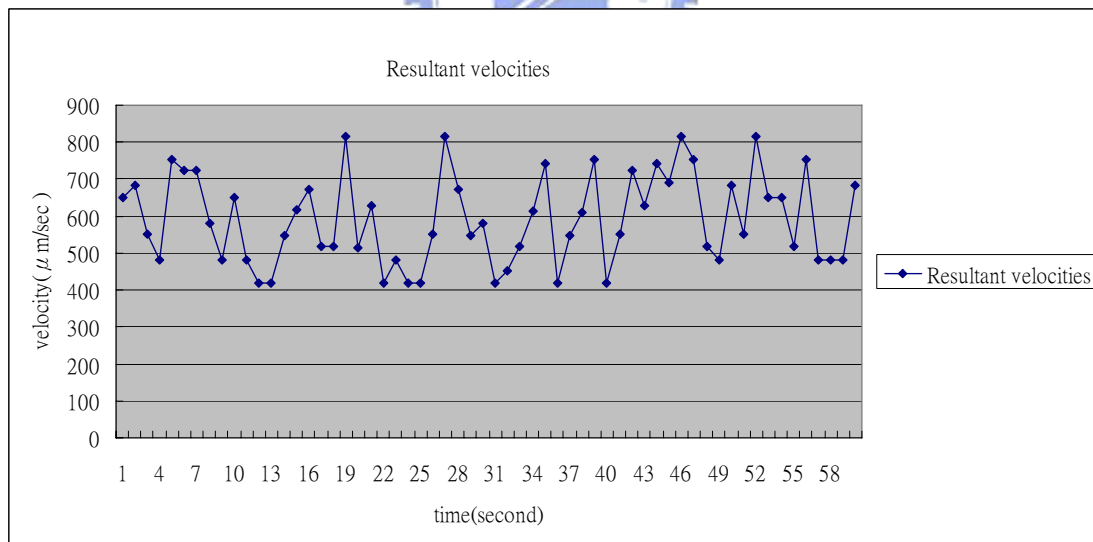


Figure 4.20 Estimate of one-minute capillary blood velocity for control subject 2.

Note that the capillary blood velocities of experimental group are much higher than that of control group. According to Liu's et al.'s study [29], practicing meditation for a long time will enhance arterial elasticity and decrease in peripheral resistance of arteries. In addition, meditation practitioners have more robust cardiovascular system than normal people. For examples, they have better ejection ability of left ventricle or aorta elasticity and better quality of semilunar valves. Besides, based on hemodynamics [30], higher blood velocity depends on less blood resistance, better elasticity of blood vessel and low blood viscosity. In sum, meditation practice might enhance the efficiency of cardiovascular system. Furthermore, higher CBV might be resulted from the decreasing peripheral resistance of the micro blood vessel, as demonstrated by hemodynamics.

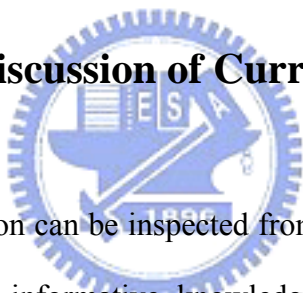


# Chapter 5

## Conclusion and Discussion

This thesis reports our study on microcirculatory phenomenon that may be a potential tool of diagnosis. Digital image instrumentation and image processing technology have been highly explored in order to estimate the capillary blood-flow velocity. At the current stage, we have come up with some concluding remarks discussed below.

### 5.1 Conclusion and Discussion of Current Study



Behaviors of microcirculation can be inspected from nailfold that is convenient for data collection and provides informative knowledge about health condition of a subject. For example, nailfold capillary blood velocity is a useful physiological parameter and diagnostic tool that has been used to validate the therapeutic effects of acupuncture. Therefore, the aim of this thesis is to develop the scheme and methodology for measuring the capillary blood velocity.

Subjects having been completed in this study are summarized below:

1. We demonstrated that G-plate component was the best choice for the preprocessing stage of capillary blood velocity analysis. Based on an inspection of histogram, the distribution of G-plate histogram is easily separated into two sections corresponding to the gray levels of the capillary and the background, respectively.



2. In regard to the issue of shifted capillary images in the microscopic video, we showed that matching all the succeeding frames to the first frame results in better performance of image realignment.
3. We showed that an image without preprocessing (ex. tuning proper gamma value, linear transform for brightness, and histogram equalization) caused a significant error in realignment.
4. The extracted skeleton of the capillary was shown to be about the centerline of the capillary. According to the centerline pattern, we have proposed three rules for choosing the centers of two observation windows.
5. We found that the capillary blood velocities of experimental group are much higher than that of control group. It is suggested that meditation practitioner might have less blood resistance, better elasticity of blood vessel and low blood viscosity.
6. We found that the capillary blood velocity reveals a phenomenon of fluctuation. And we conjecture that the cause is due to the vasomotion, and the non-uniform distribution of the blood cells.
7. For reference, we computed the capillary blood velocity by naked-eye examination (from experimental group subject 1) and we found the reference velocity is not out of range of capillary blood velocities.

In conclusion, we have presented a complete scheme for measuring the capillary blood velocity using the dual-windows method. In addition, reliability of the estimate was justified based on the scientific approach.

## 5.2 Future Work

This thesis has reported some preliminary results of investigating the microcirculatory behaviors. Although the scheme and methods have already enabled us to estimate the capillary blood velocity, there still exist some issues requiring further investigation.

1. At the preprocessing stage, the image contrast needs to be further enhanced in order to achieve better results of realignment. However, the instrument for microscopic image acquisition is limited to manual adjustment. In the future, contrast-related parameters will be adjusted and optimized automatically.
2. We may use the intensity of illumination (average of R, G, and B values) to recognize capillaries and blood flow.
3. In this thesis, the Zhang-Suen algorithm was applied to image skeletonization. Although this algorithm was computational efficient, the performance was not satisfactory that also affected the selection of centers of observation windows. As a result, it is important to develop advanced algorithm for image skeletonization.
4. Computerized automation algorithm needs to be developed for determining the observation windows.

Our research group has been investigating the Zen-meditation life system, in both physiological and mental aspects. Study on microcirculatory phenomena was originally aimed to investigate the effects caused by Zen meditation. In addition, Zen-meditation effects on microcirculatory system can be compared with those observed from other physiological signals such as heart rate variation (HRV), electrocardiograph (ECG), galvanometric skin resistance (GSR), respiratory signals,

etc.

There are two other subjects that also draw our attention.

### *1. Register the same capillary*

For long-term monitoring, it is important to always measure the capillary blood velocity for the same capillary in one subject. Accordingly, we may explore the long-term effects on microcirculatory characteristics caused by Zen meditation. We are thus looking for the possibility of registering one unique capillary.

### *2. Morphic recognition*

Health conditions of a subject can be revealed by the morphic patterns of the capillaries. In addition, microcirculatory behaviors have been used as a diagnostic reference to examine such potential diseases as 1) a connective tissue disease or macroglobulinemia signified by increasing diameters and varying contours of the capillaries, 2) low blood pressure revealed by a rapid decrease in the number of capillaries, and 3) critical infections (during the critical periods of several diseases) indicated by a slowing down or cessation of the capillary blood velocity (velocity <  $198 \mu\text{m/sec}$ ) as well as the elongation of the diameter of the capillaries. Scheme and algorithm for quantifying the capillary morphologies [31] will be developed in the future to measure the capillary diameters, to recognize their contours, to count the number, to detect hemorrhage, etc.

Finally, the nailfold capillary microscope is very important to the prediction and diagnosis of a number of diseases. Development of prognostic and diagnostic schemes significantly contributes to preventive medicine that has been in urgent need in comparison with therapeutic medicine.

# References

- [1] Aubin F., Dufour MP., Risold JC., Lucas A., Humbert P., “Nailfold capillary microscopy in human immunodeficiency virus-infected patients: a case-control study,” *Microvascular Research*, vol. 58, pp.197–199, 1999.
- [2] Martina B., Frach B., Surber C., Drewe J., Battagay E. and Gasser P., “Capillary blood cell velocity in finger nailfold: effect of Enalapril and Mibefradil in patients with mild to moderate hypertension,” *Microvascular Research*, vol.57, pp.94–99, 1998.
- [3] Brumen V., Horvat D. and Bonić I., “Evaluation of serial application of capillaroscopy, photoplethysmography, and dermothymometry in diagnosis and prevention of radiolesions of peripheral microvessels,” *Microvascular Research*, vol.47, pp.270–278, 1994.
- [4] VADER, SHERMAN, and LUCIANO, *Human Physiology*. 6<sup>th</sup> edition, McGRAW-Hill.
- [5] Stücker M., Baier V., Reuther T., Hoffmann K. and Altmeyer P., “Capillary blood cell velocity in human skin capillaries located perpendicularly to the skin surface: Measured by a new Laser Doppler Anemometer,” *Microvascular Research*, vol.52, pp. 188–192, 1996.
- [6] 李錦奎，「體表微循環量測方法與應用」，國立台灣大學，碩士論文，民國 92 年。
- [7] Norman M., Herin P. and Fagrell B., “An evaluation of skin capillary blood flow determinations in neonates using a computerized videophotometric method,” *Microvascular Research*, vol.43, pp.276–284, 1992.

- [8] 田牛，*微循環方法學*，初版，原子能出版社，1987。
- [9] 房晶萍，巨丹，线利波，「糖尿病患者微循环及血流变指标的临朧观察」，中國血液流變學雜誌，第 14 卷，第 2 期，260 頁，2004 年 6 月。
- [10] 李逸華，「影像處理於微循環檢測之研究」，國立彰化師範大學，碩士論文，民國 95 年。
- [11] 陳雪惠，「甲襞微血管影像之血流速量測分析」，私立中原大學，碩士論文，民國 91 年。
- [12] Einav S. and Berman H. J., “Fringe mode transmittance laser Doppler microscope anemometer: Its adaptation for measurement in the microcirculation,” *Biomedical Engineering*, vol.10, pp.393–399, 1988.
- [13] 易政男，「微循環顯微影像之擷取與分析」，國立中央大學，碩士論文，民國90年。
- [14] Yau H. F., Yih J. N., Lee H. Y., Lai Y. K., Chang H. H., “*In vivo* observation of the blood flow in human capillaries under finger nailfold,” *Medical and Biological Engineering*, vol.22, pp.91–96, 2002.
- [15] Intaglietta M., Silverman N. R. and Tompkins W. R., “Capillary flow velocity measurements in vivo and in situ by television methods,” *Microvascular Research*, Vol. 10, pp. 165–179, 1975.
- [16] 胡育彰，「動態影像估測之醫學影像應用」，私立中原大學，碩士論文，民國90年。
- [17] Horn K. P. and Schunck B. G., “Determining optical flow,” *Artificial Intelligence*, pp. 185–203, 1981.
- [18] Wayland H. and Johnson P. C., “Erythrocyte velocity measurement in microvessels by two-slit photometric method,” *Applied Physiology*, vol.22, pp.333–337, 1967.

- [19] Tsukada K., Minamitani H., Sekizuka E., Oshio C., “Image correlation method for measuring blood flow velocity in microcirculation: correlation ‘window’ simulation and *in vivo* image analysis,” *Physiological Measurement*, vol.21, pp.459—471, 2000.
- [20] 陳國禎，「微循環顯微觀測系統之設計製作與觀測指標模糊理論應用初步評估」，私立中原大學，碩士論文，民國90年。
- [21] Rao K. R. and Hwang J. J., *Techniques and Standards for Image, Video and Audio Coding*. Prentice Hall, 2001.
- [22] Otsu N, “A threshold selection method from gray—level histogram,” *IEEE Transactions on system, man, and cybernetics*, vol.9, pp.62—66, 1979.
- [23] Shapiro L.G. and Stockman G. C., *Computer Vision*. Upper Saddle River, N.J.: Prentice Hall, 2001.
- [24] McAndrew A., *Introduction to Digital Image Processing*. 1<sup>st</sup> edition, Thomson, 2004.
- [25] Hahn M., Heubach T., Steins A., and Jünger M., “Hemodynamics in nailfold capillaries of patients with systemic scleroderma: synchronous measurements of capillary blood pressure and red blood cell velocity,” *Investigative Dermatology*, vol.110 (6), pp.982—985, 1998.
- [26] 余麗君、姜亞芳，*病理生理學*，初版，五南圖書出版有限公司，2003。
- [27] Nelson P., *Biological Physics: Energy, Information, Life*. 1<sup>st</sup> edition, Freeman, 2004.
- [28] Carr R. T. and Lacoïn M., “Nonlinear dynamics of microvascular blood flow,” *Annals of Biomedical Engineering*, vol. 28, pp.641—652, 2000.
- [29] Liu C.Y., Wei C.C. and Lo P.C., “Variation Analysis of the Sphygmogram to Assess the Cardiovascular System under Meditation”, *Evidence-based Complementary and Alternative Medicine* (doi:10.1093/ecam/nem065).

- [30] Westerhof N., Stergiopulos N., and Noble M. I. M., *Snapshots of Hemodynamics*. Springer US, 2005.
- [31] Jones B.F., Oral M., Morris C. W., and Ring E. F. J., “A proposed taxonomy for nailfold capillaries based on their morphology,” *IEEE Transactions on Medical Imaging*, vol.20 (4), pp.333 – 341, 2004.



# Appendix A

## Other matching criteria

### 1. Sum of Absolute Difference (*SAD*)

The *SAD* is a popular measure requiring less computational time than the other methods. It is defined as

$$SAD = \sum_i \sum_j |S(i, j) - R(i, j)| \quad (A.1)$$

We denoted the reference image as  $R(i, j)$  and the other image as  $S(i, j)$ , where  $i$  and  $j$  are the pixel coordinates of the image in the image space.

### 2. Cross-correlation Coefficient (*CC*)

The cross-correlation coefficient is defined as

$$CC^2 = \frac{(\sum_i \sum_j XY - NEP \overline{XY})^2}{(\sum_i \sum_j X^2 - NEP \overline{X^2})(\sum_i \sum_j Y^2 - NEP \overline{Y^2})} \quad (A.2)$$

where  $X=S(i, j)$ ,  $Y=R(i, j)$ , and  $NEP$  is the total number of pixels included in the summation calculation.

### 3. Standard deviation of gray-level ratio (*SDGR*)

This measurement computes the standard deviation of gray-level ratio (*SDGR*). First, an  $N \times N$  ratio image,  $\text{Ratio}(i, j)$ , is derived by dividing the gray level of target image  $S(i, j)$  by the non-zero gray level of the reference image  $R(i, j)$  at the same pixel location. Then the standard deviation is computed for all the non-zero gray values in the ratio image.

$$\text{Ratio}(i, j) = \begin{cases} S(i, j) / R(i, j) & \text{if } R(i, j) \neq 0 \\ 0 & \text{if } R(i, j) = 0 \quad \forall (i, j) \end{cases} \quad (A.3)$$

and  $SDPR = \text{standard deviation of } \{ \text{Ratio}(i, j) \mid 0 \leq i, j < N \text{ and } \text{Ratio}(i, j) \neq 0 \}$



# Appendix B

## Otsu's Method:

Let the pixels of a given picture be represented in  $L$  gray levels  $[1, 2, \dots, L]$ . The number of pixels at level  $i$  is denoted by  $n_i$  and the total number of pixels by  $N = n_1 + n_2 + \dots + n_L$ . In order to simplify the discussion, the gray-level histogram is normalized and regarded as a probability distribution:

$$p_i = n_i / N \quad p_i \geq 0, \sum_{i=1}^L p_i = 1. \quad (\text{B.1})$$

Now suppose that we dichotomize the pixels into two classes  $C_0$  and  $C_1$  (background and objects) by a threshold at level  $k$ ;  $C_0$  denotes pixels with levels  $[1, \dots, k]$ , and  $C_1$  denotes pixels with levels  $[k+1, \dots, L]$ . Then the probabilities of class occurrence and the class mean levels, respectively, are given by

$$\omega_0 = \Pr(C_0) = \sum_{i=1}^k p_i = \omega(k) \quad (\text{B.2})$$

$$\omega_1 = \Pr(C_1) = \sum_{i=k+1}^L p_i = 1 - \omega(k) \quad (\text{B.3})$$

and

$$\mu_0 = \sum_{i=1}^k i \Pr(i | C_0) = \sum_{i=1}^k i p_i / \omega_0 = \mu(k) / \omega(k) \quad (\text{B.4})$$

$$\mu_1 = \sum_{i=k+1}^L i \Pr(i | C_1) = \sum_{i=k+1}^L i p_i / \omega_1 = \frac{\mu_T - \mu(k)}{1 - \omega(k)} \quad (\text{B.5})$$

where

$$\omega(k) = \sum_{i=1}^k p_i \quad (\text{B.6})$$

and

$$\mu(k) = \sum_{i=1}^k i p_i \quad (\text{B.7})$$

Are the zeroth- and the first-order cumulative moments of the histogram up to the  $k$ th level, respectively, and

$$\mu_T = \mu(L) = \sum_{i=1}^L i p_i \quad (\text{B.8})$$

is the total mean level of the original picture. It can be easily verify the following relation for any choice of  $k$ :

$$\omega_0 \mu_0 + \omega_1 \mu_1 = \mu_T, \quad \omega_0 + \omega_1 = 1 \quad (\text{B.9})$$

The class variances are given by

$$\sigma_0^2 = \sum_{i=1}^k (i - \mu_0)^2 \Pr(i | C_0) = \sum_{i=1}^k (i - \mu_0)^2 p_i / \omega_0 \quad (\text{B.10})$$

$$\sigma_1^2 = \sum_{i=k+1}^L (i - \mu_1)^2 \Pr(i | C_1) = \sum_{i=k+1}^L (i - \mu_1)^2 p_i / \omega_1 \quad (\text{B.11})$$

These require second-order cumulative moments (statistics).

In order to evaluate the “goodness” of the threshold (at level  $k$ ), Otsu introduce the following discriminant criterion measures (or measures of class separability) used in the discriminant analysis:

$$\lambda = \sigma_B^2 / \sigma_w^2, \quad \kappa = \sigma_T^2 / \sigma_w^2, \quad \eta = \sigma_B^2 / \sigma_T^2 \quad (\text{B.12})$$

where

$$\sigma_w^2 = \omega_0 \sigma_0^2 + \omega_1 \sigma_1^2 \quad (\text{B.13})$$

$$\sigma_B^2 = \omega_0 (\mu_0 - \mu_T)^2 + \omega_1 (\mu_1 - \mu_T)^2 = \omega_0 \omega_1 (\mu_1 - \mu_0)^2 \quad (\text{B.14})$$

(due to (B.9)) and

$$\sigma_T^2 = \sum_{i=1}^L (i - \mu_T)^2 p_i \quad (\text{B.15})$$

are the within-class variance, the between-class variance, and the total variance of levels, respectively. Then our problem is reduced to an optimization problem to search for a threshold  $k$  that maximizes one of the object functions (the criterion measures) in (B.12).

This standpoint is motivated by a conjecture that well-thresholded classes would be separated in gray levels, and conversely, a threshold giving the best separation of

classes in gray levels would be the best threshold.

The discriminant criteria maximizing  $\lambda$ ,  $\kappa$ , and  $\eta$ , respectively, for  $k$  are, however, equivalent to one another; e.g.,  $\kappa = \lambda + 1$  and  $\eta = \lambda / (\lambda + 1)$  in term of  $\lambda$ , because the following basic relation always holds:

$$\sigma_w^2 + \sigma_B^2 = \sigma_T^2. \quad (\text{B.16})$$

It is noticed that  $\sigma_w^2$  and  $\sigma_B^2$  are function of threshold level  $k$ , but  $\sigma_T^2$  is independent of  $k$ . It is also noted that  $\sigma_w^2$  is based on the second-order statistics (class variances), while  $\sigma_B^2$  is based on the first-order statistics (class means). Therefore,  $\eta$  is the simplest measure with respect to  $k$ . Thus Otsu adopt  $\eta$  as the criterion measure to evaluate the “goodness”(or separability) of the threshold at level  $k$ .

The optimal threshold  $k^*$  that maximizes  $\eta$ , or equivalently maximizes  $\sigma_B^2$ , is selected in the following sequential search by using the simple cumulative quantities (B.6) and (B.7), or explicitly using (B.2)-(B.5):

$$\eta(k) = \sigma_B^2(k) / \sigma_T^2 \quad (\text{B.17})$$

$$\sigma_B^2(k) = \frac{[\mu_T \omega(k) - \mu(k)]^2}{\omega(k)[1 - \omega(k)]} \quad (\text{B.18})$$

and then the optimal threshold  $k^*$  is determined by

$$\sigma_B^2(k^*) = \max_{1 \leq k < L} \sigma_B^2(k). \quad (\text{B.19})$$